The difference in cleavage patterns was not visible when the three enzymes were used to hydrolyze colloidal chitin (Fig. 6A–C). Over the first 60 min of incubation, the three enzymes essentially degraded chitin to G2 as the major product, with trace amounts of G3. Then, after 18 h, G2 and G1 were produced as the major end products, with some G3 also being present in the reaction of the W275G mutant.

The 3D-structure of *S. marcescens* chitinase A E315L mutant complexed with hexaNAG revealed that the oligosaccharide occupied subsites −4 to +2. An almost superimposition of the substrate binding clefts of *Vibrio* and *Serratia* enzymes (Fig. 2B) led to the assumption that oligosaccharide substrates would occupy the binding cleft of the *Vibrio* chitinase A in a similar manner as it was observed with the *Serratia* enzyme. Further investigation of the products released from penta- and hexaNAG hydrolyses by *S. marcescens* wild-type chitinase A demonstrated that both substrates only occupied subsites −2 to +2 with additional sugars extend beyond the substrate-binding cleft at the reducing end [22]. Such a four subsite binding mode seemed to also be the case for *B. circulans* chitinase A1 [27]. Even though the binding mode of the *Vibrio* enzyme cannot be specified at this point in time, the shift in the degradation patterns against chitooligomers upon particular point mutations gave indication that Trp275 and Trp397 are both important in the selective binding of soluble substrates.

A mutation of Trp397 to Phe results in an entire change in the cleavage patterns of the enzyme towards G6 and it can thus be assumed that Trp397 is involved in defining the primary binding sites for the incoming sugars so that the G2 and G4 will mainly be produced from the G6 substrate (Fig. 5A). Mutation of Trp397 to a less hydrophobic residue (Phe) seemed to loosen the binding affinity at this subsite. As a result, the incoming oligosaccharide had more freedom to assemble itself in the binding cleft, thus permitting various bonds to be exposed to the cleavage site (Fig. 5C). This finding is in a good agreement with the previous observations on *Serratia* and *Bacillus* chitinases [22,27]. Based on the −2 to +2 binding mode, Aronson et al. [22] suggested that the loss of binding affinity of the subsite +2 residue as a result of amino acid replacement (Trp396 to Ala) shifted the primary binding sites at least one position towards the non-reducing end.

Mutation of the +1 binding residue (Trp275) to Gly led to a major change in the hydrolysis of higher M_r oligosaccharides (as seen in Fig. 4B–D and Fig. 5B) by allowing the second and the third bonds of G6 from the non-reducing end (in the four subsite binding mode) to be equally accessed, confirming that Trp275 is involved in the specific binding of GlcNAc units around the cleavage site.

With colloidal chitin, no significant change in the cleavage patterns was seen as a result of the specific mutations of Trp275 and Trp397, which suggested that the two residues did not play the same role as in chitooligosaccharide degradation. According to "the feeding-sliding theory" suggested by Watanabe's group [23,27,34], a chitin polymer would enter the binding cleft unidirectionally from the non-reducing end rather than enter randomly like small substrates. Under these conditions, binding would be more influenced by a cluster of the surface-exposed amino acid residues that stretch along the *N*-terminal chitin binding domain through the substrate binding cleft than by particular residues.

Acknowledgements

This work was financially supported by Thailand Research Fund, The Thai Commission on Higher Education and the National Synchrotron Research Center (NSRC), Thailand. JS is a Senior Research Scholar of the Thailand Research Fund. CS was supported by a paid leave of absence from NSRC, Nakhon Ratchasima, Thailand. We would like to thank Dr. Chartchai Krittanai, Institute of Molecular Biology and Genetics, Mahidol University, Salaya, Nakhon Pathom, Thailand, for kindly providing the CD facility.

References

[1] C. Yu, A.M. Lee, B.L. Bassler, S. Roseman, Chitin utilization by marine bacteria. A physiological function for bacterial adhesion to immobilized carbohydrates, J. Biol. Chem. 266 (1991) 24260–24267.
[2] D.M. Rast, M. Horsch, R. Furter, G.W. Gooday, A complex chitinolytic system in exponentially growing mycelium of *Mucor rouxii*: properties and function, J. Gen. Microbiol. 137 (1991) 2797–2810.
[3] H. Merzendorfer, L. Zimoch, Chitin metabolism in insects: structure, function and regulation of chitin synthases and chitinases, J. Exp. Biol. 206 (2003) 4393–4412.
[4] A. Herrera-Estrella, I. Chet, Chitinases in biological control, EXS 87 (1999) 171–184.
[5] L.S. Melchers, M.H. Stuiver, Novel genes for disease-resistance breeding, Curr. Opin. Plant Biol. 3 (2000) 147–152.
[6] R.S. Patil, V.V. Ghormade, M.V. Deshpande, Chitinolytic enzymes: an exploration, Enzyme Microb. Technol. 26 (2000) 473–483.
[7] L.E. Donnelly, P.J. Barnes, Acidic mammalian chitinase—A potential target for asthma therapy, TRENDS Pharmacol. Sci. 25 (2004) 509–511.
[8] M. Wills-Karp, C.L. Karp, Chitin checking-novel insights into asthma, N. Engl. J. Med. 351 (2004) 1455–1457.
[9] W. Suginta, P.A. Robertson, B. Austin, S.C. Fry, L.A. Fothergill-Gilmore, Chitinases from *Vibrio*: activity screening and purification of chiA from *Vibrio carchariae*, J. Appl. Microbiol. 89 (2000) 76–84.
[10] W. Suginta, A. Vongsuwan, C. Songsiriritthigul, H. Prinz, P. Estibeiro, R.R. Duncan, J. Svasti, L.A. Fothergill-Gilmore, An endochitinase A from *Vibrio carchariae*: cloning, expression, mass and sequence analyses, and chitin hydrolysis, Arch. Biochem. Biophys. 424 (2004) 171–180.
[11] B. Henrissat, A. Bairoch, New families in the classification of glycosyl hydrolases based on amino acid sequence similarities, Biochem. J. 293 (1993) 781–788.
[12] A. Perrakis, I. Tews, Z. Dauter, A.B. Oppenheim, I. Chet, K.S. Wilson, C.E. Vorgias, Crystal structure of a bacterial chitinase at 2.3 Å resolution, Structure 2 (1994) 1169–1180.
[13] T. Hollis, A.F. Monzingo, K. Bortone, S. Ernst, R. Cox, J.D. Robertus, The X-ray structure of a chitinase from the pathogenic fungus *Coccidioides immitis*, Protein Sci. 9 (2000) 544–551.
[14] K. Suzuki, M. Taiyoji, N. Sugawara, N. Nikaidou, B. Henrissat, T. Watanabe, The third chitinase gene (chiC) of *Serratia marcescens* 2170 and the relationship of its product to other bacterial chitinases, Biochem. J. 343 (1999) 587–596.
[15] W. Suginta, A. Vongsuwan, C. Songsiriritthigul, J. Svasti, H. Prinz, Enzymatic properties of wild-type and active site mutants of chitinase A from *Vibrio carchariae*, as revealed by HPLC-MS, FEBS J. 272 (2005) 3376–3386.
[16] I. Tews, A.C. Terwisscha van Scheltinga, A. Perrakis, K.S. Wilson, B.W. Dijkstra, Substrate-assisted catalysis unifies two families of chitinolytic enzymes, J. Am. Chem. Soc. 119 (1997) 7954–7959.

[17] K.A. Brameld, W.A. Goddard III, Substrate distortion to a boat conformation at subsite −1 is critical in the mechanism of family 18 chitinases, J. Am. Chem. Soc. 120 (1998) 3571–3580.
[18] A.C. Terwisscha van Scheltinga, S. Armand, K.H. Kalk, A. Isogai, B. Henrissat, B.W. Dijkstra, Stereochemistry of chitin hydrolysis by a plant chitinase/lysozyme and X-ray structure of a complex with allosamidin: evidence for substrate assisted catalysis, Biochemistry 34 (1995) 15619–15623.
[19] D.M. van Aalten, D. Komander, B. Synstad, S. Gaseidnes, M.G. Peter, V.G. Eijsink, Structural insights into the catalytic mechanism of a family 18 exo-chitinase, Proc. Natl. Acad. Sci. U. S. A. 98 (2001) 8979–8984.
[20] C. Sasaki, A. Yokoyama, Y. Itoh, M. Hashimoto, T. Watanabe, T. Fukamizo, Comparative study of the reaction mechanism of family 18 chitinases from plants and microbes, J. Biochem. (Tokyo) 131 (2002) 557–564.
[21] T. Fukamizo, C. Sasaki, E. Schelp, K. Bortone, J.D. Robertus, Kinetic properties of chitinase-1 from the fungal pathogen *Coccidioides immitis*, Biochemistry 40 (2001) 2448–2454.
[22] N.N. Aronson Jr., B.A. Halloran, M.F. Alexyev, L. Amable, J.D. Madura, L. Pasupulati, C. Worth, P. Van Roey, Family 18 chitinase-oligosaccharide substrate interaction: subsite preference and anomer selectivity of *Serratia marcescens* chitinase A, Biochem. J. 376 (2003) 87–95.
[23] T. Watanabe, A. Ishibashi, Y. Ariga, M. Hashimoto, N. Nikaidou, J. Sugiyama, T. Matsumoto, T. Nonaka, Trp122 and Trp134 on the surface of the catalytic domain are essential for crystalline chitin hydrolysis by *Bacillus circulans* chitinase A1, FEBS Lett. 494 (2001) 74–78.
[24] T. Uchiyama, F. Katouno, N. Nikaidou, T. Nonaka, J. Sugiyama, T. Watanabe, Roles of the exposed aromatic residues in crystalline chitin hydrolysis by chitinase A from *Serratia marcescens* 2170, J. Biol. Chem. 276 (2001) 41343–41349.
[25] F. Katouno, M. Taguchi, K. Sakurai, T. Uchiyama, N. Nikaidou, T. Nonaka, J. Sugiyama, T. Watanabe, Importance of exposed aromatic residues in chitinase B from *Serratia marcescens* 2170 for crystalline chitin hydrolysis, J. Biochem. (Tokyo) 136 (2004) 163–168.
[26] Y. Itoh, J. Watanabe, H. Fukada, R. Mizuno, Y. Kezuka, T. Nonaka, T. Watanabe, Importance of Trp59 and Trp60 in chitin-binding, hydrolytic, and antifungal activities of *Streptomyces griseus* chitinase C, Appl. Microbiol. Biotechnol. 72 (2006) 1176–1184.
[27] T. Watanabe, Y. Ariga, U. Sato, T. Toratani, M. Hashimoto, N. Nikaidou, Y. Kezuka, T. Nonaka, J. Sugiyama, Aromatic residues within the substrate-binding cleft of *Bacillus circulans* chitinase A1 are essential for hydrolysis of crystalline chitin, Biochem. J. 376 (2003) 237–244.
[28] Collaborative Computational Project, Number 4, The CCP4 suit: programs for protein crystallography, Acta Cryst. D50 (1994) 760–763.
[29] U.K. Laemmli, Cleavage of structural proteins during the assembly of the head of bacteriophage T4, Nature 227 (1970) 680–685.
[30] M.M. Bradford, A rapid and sensitive method for the quantitation of microgram quantities of protein utilizing the principle of protein-dye binding, Anal. Biochem. 72 (1976) 248–254.
[31] A. Bruce, U. Srinivasan, H.J. Staines, T.L. Highley, Chitinase and laminarinase production in liquid culture by *Trichoderma* spp. and their role in biocontrol of wood decay fungi, Int. Biodeterior. Biodegrad. 35 (1995) 337–353.
[32] S.C. Hsu, J.L. Lockwood, Powdered chitin agar as a selective medium for enumeration of actinomycetes in water and soil, Appl. Microbiol. 29 (1975) 422–426.
[33] T. Tanaka, S. Fujiwara, S. Nishikori, T. Fukui, M. Takagi, T. Imanaka, A unique chitinase with dual active sites and triple substrate binding sites from the hyperthermophilic Archaeon *Pyrococcus kodakaraensis* KOD1, Appl. Environ. Microbiol. 15 (1999) 5338–5344.
[34] T. Imai, T. Watanabe, T. Yui, J. Sugiyama, Directional degradation of beta-chitin by chitinase A1 revealed by a novel reducing end labelling technique, FEBS Lett. 510 (2002) 201–205.
[35] N.N. Aronson Jr., B.A. Halloran, M.F. Alexeyev, X.E. Zhou, Y. Wang, E.J. Meehan, L. Chen, Mutation of a conserved tryptophan in the chitin-binding cleft of *Serratia marcescens* chitinase A enhances transglycosylation, Biosci. Biotechnol. Biochem. 70 (2006) 243–251.

BMC Biochemistry

BioMed Central

Research article

Open Access

The effects of the surface-exposed residues on the binding and hydrolytic activities of *Vibrio carchariae* chitinase A

Supansa Pantoom[1], Chomphunuch Songsiriritthigul[2] and Wipa Suginta*[1]

Address: [1]School of Biochemistry, Suranaree University of Technology, Nakhon Ratchasima 30000, Thailand and [2]National Synchrotron Research Center, Nakhon Ratchasima 30000, Thailand

Email: Supansa Pantoom - aon_biochem@hotmail.com; Chomphunuch Songsiriritthigul - pook@nsrc.or.th; Wipa Suginta* - wipa@sut.ac.th

* Corresponding author

Published: 21 January 2008

BMC Biochemistry 2008, **9**:2 doi:10.1186/1471-2091-9-2

Received: 17 September 2007
Accepted: 21 January 2008

This article is available from: http://www.biomedcentral.com/1471-2091/9/2

Abstract

Background: *Vibrio carchariae* chitinase A (EC3.2.1.14) is a family-18 glycosyl hydrolase and comprises three distinct structural domains: i) the amino terminal chitin binding domain (ChBD); ii) the $(\alpha/\beta)_8$ TIM barrel catalytic domain (CatD); and iii) the $\alpha + \beta$ insertion domain. The predicted tertiary structure of *V. carchariae* chitinase A has located the residues Ser33 & Trp70 at the end of ChBD and Trp231 & Tyr245 at the exterior of the catalytic cleft. These residues are surface-exposed and presumably play an important role in chitin hydrolysis.

Results: Point mutations of the target residues of *V. carchariae* chitinase A were generated by site-directed mutagenesis. With respect to their binding activity towards crystalline α-chitin and colloidal chitin, chitin binding assays demonstrated a considerable decrease for mutants W70A and Y245W, and a notable increase for S33W and W231A. When the specific hydrolyzing activity was determined, mutant W231A displayed reduced hydrolytic activity, whilst Y245W showed enhanced activity. This suggested that an alteration in the hydrolytic activity was not correlated with a change in the ability of the enzyme to bind to chitin polymer. A mutation of Trp70 to Ala caused the most severe loss in both the binding and hydrolytic activities, which suggested that it is essential for crystalline chitin binding and hydrolysis. Mutations varied neither the specific hydrolyzing activity against *p*NP-$[GlcNAc]_2$, nor the catalytic efficiency against chitohexaose, implying that the mutated residues are not important in oligosaccharide hydrolysis.

Conclusion: Our data provide direct evidence that the binding as well as hydrolytic activities of *V. carchariae* chitinase A to insoluble chitin are greatly influenced by Trp70 and less influenced by Ser33. Though Trp231 and Tyr245 are involved in chitin hydrolysis, they do not play a major role in the binding process of crystalline chitin and the guidance of the chitin chain into the substrate binding cleft of the enzyme.

Background

Chitin is a homopolysaccharide chain of *N*-acetylglucosamine (GlcNAc or G1) units combined together with β-1,4 glycosidic linkages. Chitin is one of the most abundant biopolymers found in nature as constituent of fungal cell walls and exoskeletons of crustaceans and insects. However, the β-GlcNAc units that generally form intra- and intermolecular H-bonds make chitin completely insoluble in water and its use is thus limited. Several strategies have been developed for converting chitin into small

soluble derivatives, which are more useful for applications in the fields of medicine, agriculture and industry. Enzymatic degradation of chitin using biocatalysts seems to be the method of choice since the type, quantity and quality of oligomeric products can be well controlled and the reaction occurs quickly and completely under mild conditions without generation of environmental pollutants.

Chitinases (EC3.2.1.14) are a diverse group of enzymes that catalyze the conversion of insoluble chitin to soluble oligosaccharides. They are found in a wide variety of organisms including virus, bacteria, fungi, insects, plants and animals [1-8]. In the carbohydrate active enzymes (CAZy) database http://www.cazy.org/, carbohydrate enzymes are first classified as glycosyl hydrolases (GH), glycosyl transferases (GT), polysaccharide lyases (PL), carbohydrate esterases (CE), and carbohydrate binding modules (CBM), and then further divided into numbered families with structurally-related catalytic and carbohydrate-binding modules. Following this classification, chitinases are commonly listed as family GH-18 and family GH-19 enzymes. Family-18 chitinases have the catalytic crevice located at top of the $(\alpha/\beta)_8$-TIM barrel domain [9,10], whereas the catalytic domain of family-19 chitinases comprises two lobes, each of which is rich in α-helical structure [11]. Bacteria such as *Serratia marcescens*, *Bacillus circulans*, *Alteromonas sp*. and marine *Vibrios* produce chitinases to synergistically degrade chitin and use it as a sole source of energy [1,12-16]. The mechanism of chitin degradation by bacterial chitinases was mainly derived from the outcome of structural studies or site-directed mutagenesis [17-20]. Unlike chitooligosaccharides, chitin polymer has been presumed to unidirectionally enter the substrate binding cleft of chitinases under the guidance of a few surface-exposed residues at the exterior of the substrate binding cleft [21,22]. Those residues were identified as Trp33, Trp69, Phe232, and Trp245 in *S. marcescens* Chi A [18], Ser33, Trp70, Trp232, and Trp245 in *Aeromonas caviae* Chi1 [23], and Trp122 and Trp134 in *B. circulans* Chi A1 [17]. Structurally, the latter two residues are located in the equivalent locations of Tyr245 and Trp231, respectively of *V. carchariae* chitinase A (Fig. 1 and ref [17]). We previously isolated chitinase A from a marine bacterium, *Vibrio carchariae* [24]. The enzyme was found to be highly expressed upon induction with chitin and was active as a monomer of 63 kDa. The DNA fragment encoding the functional chitinase A was subsequently cloned into the pQE60 expression vector that was compatible to be highly expressed in *E. coli* type strain M15 [25]. Mutational studies confirmed that the conserved Glu315 acts as the catalytic residue in the substrate-assisted mechanism [26,27], whereas the aromatic residues including Trp168, Tyr171, Trp275, Trp397 and Trp570 participated in direct interactions with chitooligosaccharides [28]. In this study, site-directed mutagenesis was employed in combination with following chitin binding assays and kinetic analysis to investigate the significance of the putative surface-exposed residues Ser33, Trp70, Trp231 and Tyr245 for the binding and hydrolytic activities of the *Vibrio* chitinase A.

Results

Homology modeling and sequence analysis

We previously reported gene isolation and sequence analysis of *V. carchariae* chitinase A precursor [25]. Site-directed mutation of the active site residues showed that Glu315 plays an essential role in catalysis [26]. On the other hand, the conserved aromatic residues (Trp168, Tyr171, Trp275, Trp397 and Trp570) located within the substrate binding cleft of the enzyme were found to be important in binding to chitooligosaccharides [28]. Here, we have investigated the functional roles of four amino acid residues (Ser33, Trp70, Trp231 and Tyr245) at the surface of *V. carchariae* chitinase A. All of these residues have been proposed as functionally relevant to binding and hydrolysis of crystalline chitin [17,18]. Fig. 1 represents the modeled 3D-structure of *V. carchariae* chitinase A that was built based upon the crystal structure of *S. marcescens* chitinase A mutant E315L complexed with a chitohexamer [see Methods]. It can clearly be seen that the four residues linearly align with each other. Trp70 and Ser33 are positioned at the end of the *N*-terminal chitin binding domain (ChBD), whilst Trp231 and Tyr245 are found outside the substrate binding cleft where they are part of the TIM barrel catalytic domain.

When the amino acid sequences of several bacterial chitinases were compared, the *V. carchariae* chitinase A (Q9AMP1) exhibited highest sequence identity with chitinase A from *V. harveyi* HY01 (A6AUU6) (93%), moderate identity with chitinase A from *S. marcescens* (P07254) and *Enteromonas sp*. (Q4PZF3) (47%), and low identity with chitinase A1 from *B. circulans* (22%). Surprisingly, extremely low sequence identity was observed when *V. carchariae* chitinase A was compared with chitinase A from *V. splendidus* (A3UMC6) (13%) and *V. cholerae* (A6ACY6) (11%).

A structure-based alignment of three chitinases, including *V. carchariae* chitinase A, *S. marcescens* chitinase A, and *B. circulans* WL-12 chitinase A1 was constructed and is displayed in Fig. 2A &2B. Fig. 2A represents an alignment of the *N*-terminal ChBDs of the *Vibrio* and *Serratia* chitinases with the *C*-terminal fragment that covers the ChBD of the *Bacillus* chitinase A1 ($ChBD_{chiA1}$). The $ChBD_{chiA1}$consists of the residues 655 to 699 and deletion of this domain led to a severe loss in the binding activity to chitin as well as in the colloidal chitin-hydrolyzing activity, suggesting that this domain is essential for binding to insoluble chitin of this enzyme [29]. As shown in Fig. 2A, the residues

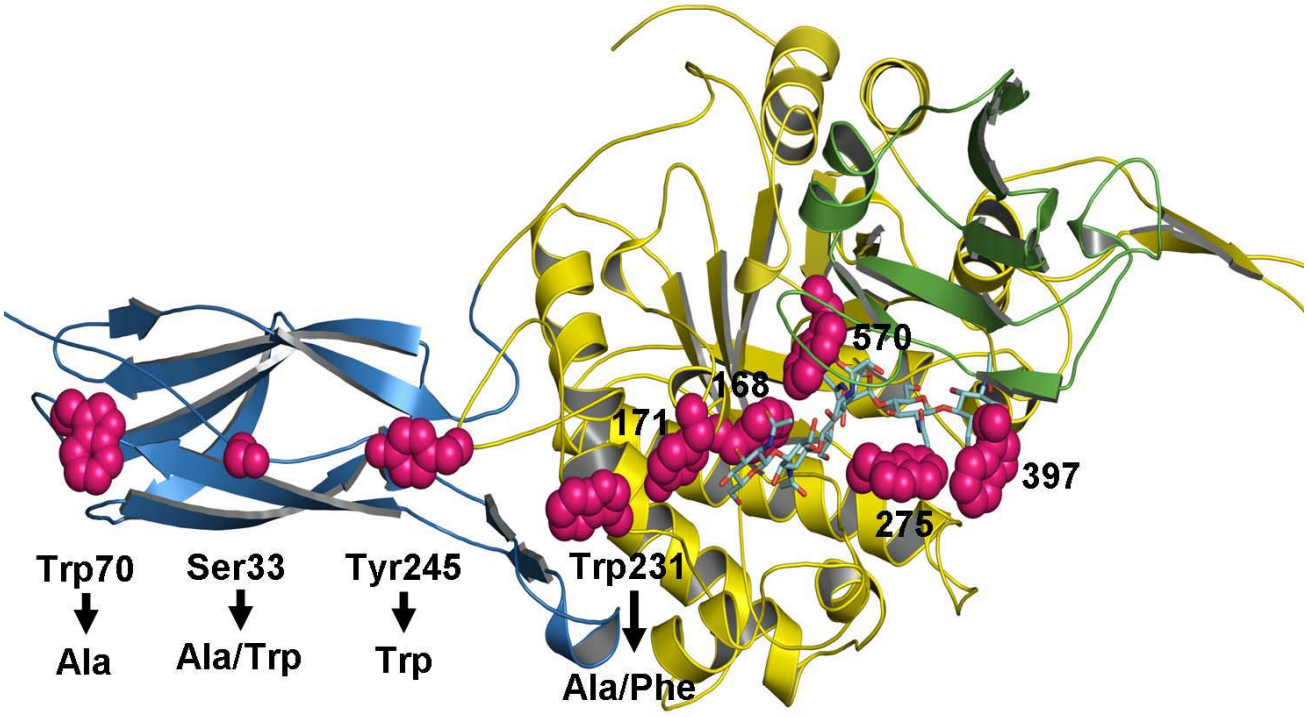

Figure 1
The Swiss-Model 3D-structure of *V. carchariae* chitinase A. A ribbon representation of the 3D-structure of *V. carchariae* chitinase A was constructed based on the x-ray structure of *S. marcescens* Chi A E315L mutant as described in the text. The *N*-terminal chitin binding domain is presented in cyan, the TIM barrel domain in yellow and the small insertion domain in green. The coordinates of $[GlcNAc]_6$ that are modeled in the active site of the *Vibrio* enzyme are shown as a stick model with N atoms in blue and O atoms in red. The mutated residues (Ser33, Trp70, Trp231 and Tyr245) and other substrate binding residues are also presented in stick model (magenta).

Trp656 and Trp687 of the $ChBD_{chiA1}$ are well aligned with Ser33 and Trp70 of *V. carchariae* chitinase A. However, the determination of the solution structure of the $ChBD_{chiA1}$ by Ikegami et al. [30] identified only Trp687 as a putative chitin binding residue, in addition to His681, Thr682, Pro689, and Pro693.

With respect to the alignment of the catalytic domain (Fig. 2B), Trp231 of the *Vibrio* chitinase is equivalent to Trp122 and to Phe232 of the *Bacillus* and *Serratia* chitinases. For Tyr245, this residue is replaced by Trp134 and Trp245 in the *B. circulans* and *S. marcescens* sequences, respectively. The sequence alignment additionally demonstrates the residues Ser33 and Trp70 within the flexible loops that join two strands in the chitin binding region. The residues Trp245 and Tyr231 are found as part of the catalytic $(\alpha/\beta)_8$ TIM barrel, where Tyr245 is exposed on the loop that joins helices 2(3) and 2(4) together and Trp231 is the only residue being found in an α-helix (helix 2(3)).

Expression and purification of chitinase A and mutants

To investigate the binding and hydrolytic activities of *V. carchariae* chitinase A, target residues as named above were mutated by sited-directed mutagenesis. According to the employed system, the recombinant chitinases were expressed as the *C*-terminally $(His)_6$ tagged fusion protein (see Methods). After single-step purification using Ni-NTA agarose affinity chromatography, the yields of the purified proteins was estimated to be approx. 20 to 25 mg/ml per litre of bacterial culture. As analyzed by SDS-PAGE, all the mutated proteins displayed a single band of molecular weight of 63 kDa (data not shown), which is identical to the molecular weight of the wild-type enzyme.

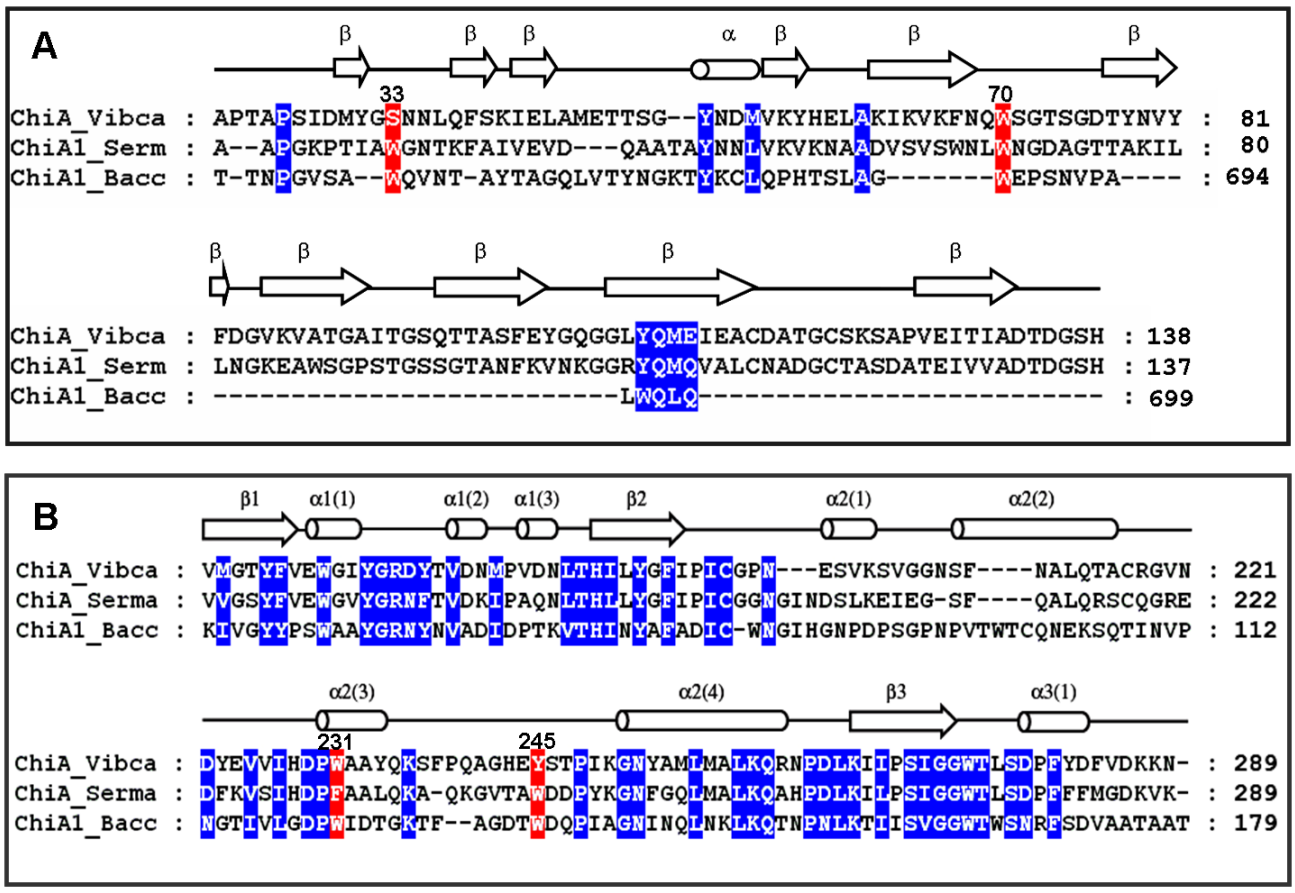

Figure 2

A structure-based alignment of *V. carchairae* chitinase A with *S. marcescens* chitinase A and *B. circulans* chitinase A1. A) The *N*-terminal ChBDs of *V. carchariae* chitinase A (residues 22–138) and *S. marcescens* chitinase A (residues 24–137) were aligned with the *C*-terminal fragment (residues 648–699), covering the ChBD of *B. circulans* WL-12 chitinase A1. B) An alignment of the catalytic domain of the three bacterial chitinases with residues 160 to 289 of *V. carchariae* chitinase A being displayed. The chitinase sequences were retrieved from the Swiss-Prot/TreEMBL protein databases, aligned using "MegAlign" in the DNASTAR package, and displayed in Genedoc. The secondary structure of *V. carchariae* chitinase A was predicted from the PHD method in PredictProtein using *S. marcescens* as template [see texts]. Conserved residues are shaded in blue, whereas the residues that are aligned with Ser33, Trp70, Trp231, and Tyr245 of *V. carchariae* chitinase A are shaded in red. ChiA_Vibca: *V. carchariae* chitinase A (Q9AMP1), ChiA_Serma: *S. marcescens* chitinase A (P07254), and ChiA1_Bacc: *B. circulans* chitinase A1 (P20533). β-strand is represented by an arrow, α-helix by a cylinder and loop by a straight line.

Effects of mutations on the chitin binding activities of chitinase A

To minimize hydrolysis, all the binding experiments were carried out on ice. Bindings of the wild-type chitinase and mutants to colloidal chitin were initially investigated as a function of time. After a removal of the enzyme bound to chitin, decreases in concentration of the unbound enzyme remaining in the supernatant was monitored discretely at different time points of 0 to 120 min. Fig. 3 demonstrates that the binding process took place rapidly and reached equilibrium within 5 min. The relative binding activity of each mutant to colloidal chitin is following the order W231A > S33W > WT ≅ W231F > S33A > Y245W > W70A. The binding activity of the individual mutants relative to the one of the wild-type enzyme was further examined with colloidal chitin and α-chitin polysaccharides at a single time point of 60 minutes. In general, the wild-type and mutant chitinases expressed greater binding activity towards colloidal chitin. A comparison of the level of binding of the engineered enzymes to the two substrates revealed a similar pattern (Fig. 4). For both polysaccharides, W70A and Y245W displayed lower binding activity than the wild-type enzyme. S33A and W231F showed a modest increase in binding to crystalline α-chitin and decreased level of binding to colloidal chitin. Mutants S33W and W231A, on the other hand, displayed higher

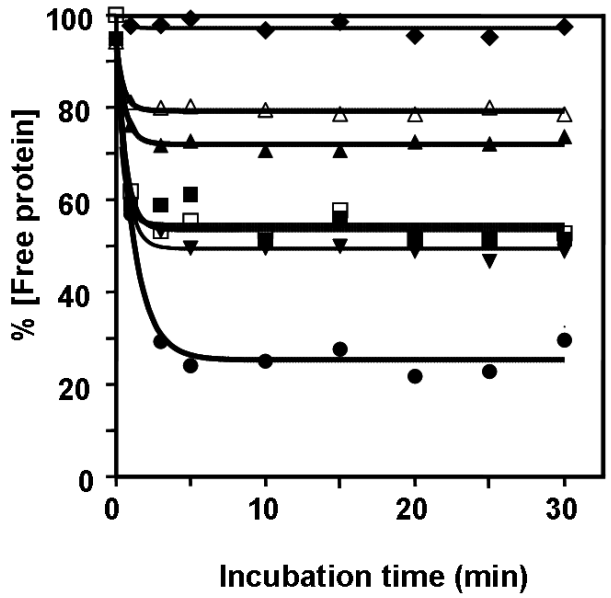

Figure 3
Time-course of binding of chitinase A and mutant enzymes to colloidal chitin. Chitinases (1 μmol in 100 mM sodium acetate buffer, pH 5.5) were incubated with 1.0 mg colloidal chitin at 0°C. Decreases in free enzyme concentration were determined at different time points from 0–30 min by Bradford's method. Each data value was calculated from triplicate experiments. Symbols: wild-type (black square); S33A (black upward-pointing triangle); S33W (black downward-pointing triangle); W70A (black diamond); W231A (black circle); W231F (open square); and Y245W (open triangle).

effectiveness in the binding to both substrates. Of all, mutant W231A displayed highest binding activity and W70A exhibited lowest activity. Especially, no detectable binding to crystalline α-chitin was observed with mutant W70A.

Adsorption isotherms of chitinase mutants to colloidal chitin were carried out relative to that of the wild-type enzyme. Fig. 5 represents a non linear plot of the adsorption isotherms obtained at a fixed concentration of colloidal chitin but varied concentrations of the enzyme (See Methods). In comparison to the wild-type enzyme, mutants S33W and W231A exhibited significantly higher binding activity, whereas mutants W70A, S33A, W231F and Y245W had a notably decreased binding activity. When the dissociation binding constants (K_d) were estimated from the non-linear regression function, it was found that the K_d value of wild-type (0.95 ± 0.11 μM) was slightly larger than the K_d values of S33W (0.84 ± 0.09 μM) and W231F (0.88 ± 0.09 μM), but remarkably greater than the value of W231A (0.26 ± 0.03 μM). In contrast, significantly higher K_d values than the wild-type value were observed with S33A (1.50 ± 0.11 μM), W70A (2.30 ± 0.25 μM), and Y245W (1.60 ± 0.16 μM). These estimated K_d values gave a notation of the enzyme's binding strength in the following order W231A > S33W > W231F > wild-type > S33A > Y245W > W70A, which is in absolute accordance with the binding activities determined by the chitin binding assay (see Fig. 4) and the kinetic data as described below.

Effects of mutations on the hydrolytic activities of chitinase A

The effects of mutations on the hydrolytic activity of *V. carchariae* chitinase A were further studied by exposing the wild-type and modified enzymes to *p*NP-$[GlcNAc]_2$, colloidal chitin and crystalline α-chitin. The specific hydrolyzing activity for the three different substrates was subsequently determined. From all the mutants, only W231A displayed a slightly reduced specific hydrolyzing activity against the *p*NP substrate (Table 1).

Unlike the *p*NP-glycoside, strong effects on the hydrolytic activities were observed with the insoluble polymeric substrates. The hydrolyzing activity against crystalline α-chitin was completely abolished in case of mutants S33A, W70A and W231A/F but improved for mutants S33W and Y245W at levels of 166% and 250% of the wild-type activity, respectively. A similar trend was also seen with colloi-

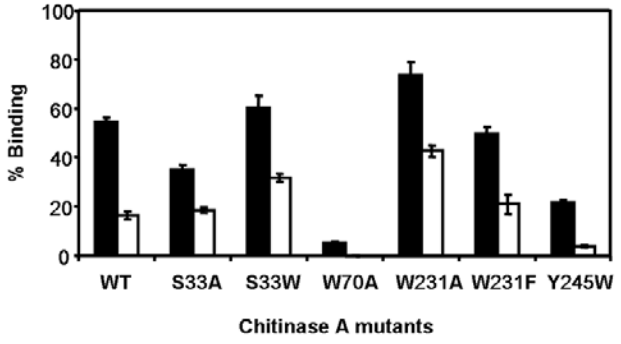

Figure 4
Binding of chitinase A and mutants to insoluble chitin. The binding assay set as described in the text was incubated with crystalline α-chitin or colloidal chitin for 60 min. The % binding = $\left[\frac{E_t - E_f}{E_t}\right] \times 100$; where E_t is initial enzyme concentration and E_f is the free enzyme concentration after binding. Closed and open bars represent % binding to colloidal chitin and crystalline α-chitin, respectively. The presented data are mean values obtained from three independent sets of the experiment.

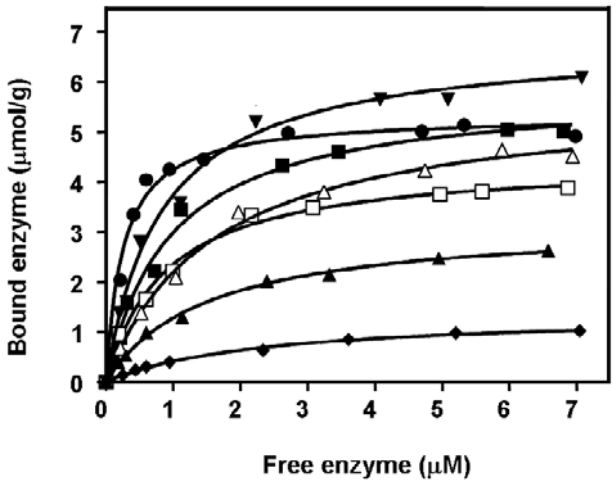

Figure 5
Equilibrium adsorption isotherms of wild-type and mutant chitinases A to colloidal chitin. The reaction assay (500 μl) contained 1.0 mg chitin and varied concentrations of enzyme from 0 to 7.0 μM. After 60 min of incubation at 0°C, the reaction mixture was centrifuged and concentrations of E_b and E_f were determined as described in the text. Symbols: wild-type (black square); S33A (black upward-pointing triangle); S33W (black downward-pointing triangle); W70A (black diamond); W231A (black circle); W231F (open square); and Y245W (open triangle).

dal chitin. However, for this substrate S33A, W70A and W231A/F not completely abolished but markedly decreased hydrolyzing activity, while S33W (119%) and Y245W (152%) again where the ones that displayed higher activity than wild-type enzyme. The most severe loss of the specific hydrolyzing activity towards colloidal chitin was detected for mutant W70A, which had a substitution of Trp70 to Ala.

Steady-state kinetics of chitinase A and mutants

The kinetic parameters of the hydrolytic activity of chitinase A and mutants were finally determined with chitohexaose and colloidal chitin as substrates. As presented in Table 2, mutations of the chosen residues led for the response of enzyme values towards the hexachitooligomer to concomitant decreases in both the K_m and k_{cat} values. For all the mutants, however, the overall catalytic efficiency (k_{cat}/K_m) was not much different to the value observed for the wild-type enzyme. In contrast, the kinetic properties of the enzyme against colloidal chitin were significantly modified by the mutations. The K_m values of S33A (2.07 10^1 mg ml^{-1}), W70A (2.26 10^1 mg ml^{-1}), and Y245W (1.82 10^1 mg ml^{-1}) were higher than the wild-type K_m (1.74 10^1 mg ml^{-1}) whereas S33W (1.58 10^1 mg ml^{-1}) and W231A (1.01 10^1 mg ml^{-1}) had considerably lower K_m compared to the reference value. Mutations that caused a large decrease in the enzyme's catalytic activity, k_{cat}, were Ser33 to Ala, Trp70 to Ala and Trp231 to Ala/Phe, whereas mutations of Ser33 to Trp and Tyr245 to Trp elevated k_{cat} values instead. The overall catalytic efficiency (k_{cat}/K_m) that was calculated for the hydrolysis of colloidal chitin was to more or less extent either reduced (for S33A, W70A, W231A and W231F) or increased (for S33W and Y245W).

Discussion

This study describes the possible role of Ser33, Trp70, Trp231, and Tyr245 in chitin binding and hydrolysis. Point mutations of these residues were introduced by site-directed mutagenesis and changes in the binding and hydrolytic activities of the enzyme as a result of the amino acid substitution were subsequently investigated for various substrates. Chitin binding assays (Fig. 3 &4) demonstrate a decrease in the binding activity of mutants S33A, W70A and Y245W to various extents. However, the most severe effect was observed with W70A. A time course study displayed no binding activity of W70A but retained activ-

Table 1: Specific hydrolyzing activity of chitinase A and mutants. The reducing sugar assay was carried out against crystalline and colloidal chitin. The release of the hydrolytic products was calculated from a standard curve of $[GlcNAc]_2$. On the other hand, the specific hydrolyzing activity against *p*NP-$[GlcNAc]_2$ was determined by the colorimetric assay. The release of *p*NP was estimated from a standard curve of *p*NP

Protein	Specific hydrolyzing activity (U/μmol protein)[a]		
	Crystalline chitin	Colloidal chitin	*p*NP-$[GlcNAc]_2$
Wild-type	0.59 ± 0.02(100)[b]	12.9 ± 0.22 (100)	50.5 ± 1.13 (100)
S33A	n.d.[c]	8.5 ± 0.50 (66)	58.0 ± 1.08 (115)
S33W	1.00 ± 0.08 (166)	15.3 ± 0.32 (119)	54.0 ± 2.55 (107)
W70A	n.d.	4.3 ± 0.17 (33)	52.8 ± 2.14 (105)
W231A	n.d.	6.6 ± 0.26 (51)	45.2 ± 2.00 (90)
W231F	n.d.	9.2 ± 0.49 (71)	54.3 ± 2.85 (108)
Y245W	1.49 ± 0.09 (250)	19.6 ± 0.53 (152)	53.6 ± 1.61 (106)

[a] One unit of chitinase is defined as the amount of enzyme that releases 1 μmol of $[GlcNAc]_2$ or 1 nmol of *p*NP per min at 37°C.
[b] Values in parentheses represent relative specific hydrolyzing activities (%).
[c] Non-detectable activity.

Table 2: Kinetic parameters of substrate hydrolysis by chitinase A wild-type and mutants. A kinetic study was carried out using 0–5% (w/v) colloidal chitin and 0–500 μM chitohexaose as substrates. After 10 minutes of incubation at 37°C, the amounts of the reaction products were determined from a standard curve of $[GlcNAc]_2$

Chitinase A variant	Chitohexaose			Colloidal chitin		
	K_m(μM)	k_{cat} (s^{-1})	k_{cat}/K_m($s^{-1}M^{-1}$)	K_m(10^1 mg ml^{-1})	k_{cat} (s^{-1})	k_{cat}/K_m(10^{-1} s^{-1}/ mg ml^{-1})
Wild-type	218 ± 22.0	2.9	1.3×10^3 (100)[a]	1.74 ± 0.1	1.2	0.7 (100)
S33A	171 ± 20.5	2.6	1.5×10^3 (115)	2.07 ± 0.2	0.9	0.4 (57)
S33W	210 ± 15.4	2.8	1.3×10^3 (100)	1.58 ± 0.2	1.4	0.9 (129)
W70A	185 ± 22.0	2.5	1.3×10^3 (100)	2.26 ± 0.4	0.4	0.2 (29)
W231A	189 ± 13.2	2.6	1.4×10^3 (108)	1.01 ± 0.2	0.6	0.6 (86)
W231F	163 ± 10.3	2.4	1.5×10^3 (115)	1.70 ± 0.2	0.9	0.5 (71)
Y245W	201 ± 13.1	2.6	1.3×10^3 (100)	1.82 ± 0.2	1.7	0.9 (129)

[a] Relative catalytic efficiencies (%) are shown in parentheses.

ity of other mutants to colloidal chitin (Fig. 3). This strongly suggested that Trp70 is the major determinant for insoluble chitin binding. Sugiyama and colleagues previously employed the reducing-end labeling technique and the tilt micro-diffraction method [21,22] to illustrate the molecular directionality of crystalline β-chitin hydrolysis by *S. marescens* chitinase A and *B. chitinase* chitinase A1. If the chitin polymer enters the substrate binding cleft of *V. carchariae* chitinase A from the reducing end as described for the *Serratia* and *Bacillus* enzymes, Trp70 will likely serve as a platform for the arrival of a chitin molecule. This idea is well complimented by the location of the residue at the end of ChBD. A remarkable loss of the specific hydrolyzing activity as well as the decrease in the rate of enzyme turnover (k_{cat}) that was observed for mutant W70A is hence explainable by the loss of the binding strength due to a substitution of Trp to Ala and an associated change in the hydrophobic interactions. A similar performance was seen for residue Ser33. Although to a lesser extent, a mutation of Ser33 to Ala also led to decreased binding activity, while its mutation to Trp improved binding activity. This finding provides additional evidence that binding of the chitin chain to the ChBD is cooperatively taken place via hydrophobic interactions and influenced by the molecular setting in this region.

The most striking observations were made with the residue Trp231. As demonstrated by the modeled 3D-structure (see Fig. 1), the residue Trp231 is placed at the outermost of the catalytic surface, thereby lying closest to the non-reducing end of the substrate binding cleft. The observed drastic improvement (rather than reduction) in the binding efficiency of mutant W231A could only be explained as a removal of the side-chain blockage. Hence, the reduced hydrolyzing activity of mutant W231A was unlikely influenced by changes in the binding acitivity as a result of the alanine substitution of Trp231. Apparently, the same phenomenon was previously recognized in *S. marcescens* chitinase A [18], with which a mutation of Phe232 to Ala seriously diminished the hydroyzing acitivty but left the binding activities to both colloidal chitin and β-chitin microfibrils unchanged.

When the next residue in line (Tyr245) (see Fig. 1) was mutated to a bulkier side-chain (Trp), inverse effects (reduced binding but improved hydrolysis) were observed. This complimented the idea of the binding barrier around the entrance hall of the catalytic domain by Trp231 and Tyr245. Similar findings were also recognized with a cellulose degrading enzyme, *Thermobifida fusca* endoglucanase (Cel9A) [31]. With this enzyme, it was observed that mutations of the surface-exposed cellulose binding residues Arg557 and Glu559 to Ala (mutant R557A/E559A) led to a severe loss in the hydrolytic activity against crystalline cellulose, but a change in the binding activity was not at all observed. Structurally, the residues Arg557 and Glu559 are found on the surface of the cellulose binding module (CBM), closest to the catalytic binding cleft of Cel9A. Therefore, the effects of Arg557 and Glu559 would be explained in analogy to those of Trp231 and Tyr245 in *V. carchariae* chitinase A.

In marked contrast, observations made with the *Vibrio* Trp231 mutation were different to the studies of Li et al. on *A. caviae* Chi 1 [23] and of Watanabe et al. on *B. circulans* Chi A1 [17]. Mutations of Trp232 and Trp245 (in *A. caviae* Chi 1) or Trp122 and Trp 134 (in *B. circulans*) to alanine resulted in a marked loss in both binding and hydrolyzing acitivities, especially againts crystalline β-chitin. Therefore, the reduced hydrolytic activities were assumed to be associated with the weaker binding of the two corresponding residues. Based on their mutational data, the residues seemed to participate directly in binding

to crystalline chitin, and subsequently cooperatively assisting the chitin chain to penetrate through the catalytic cleft of *A. caviae* or *B. circulans* chitinase.

Indeed, the above-mentioned event that took place in the *A. carviae* and *B. circulans* chitinases did not seem to be the case for the *V. carchariae* chitinase A due to different behaviors of Trp231 and Tyr245 found for the *Vibrio* enzyme. Our data suggested that a possible action of *V. carchariae* chitinase A on insoluble chitin could proceed as follows: i) Initial binding of a chitin chain to the ChBD. This process is most influenced by the hydrophobic interaction set between the incoming sugar and residue Trp70, which is located at the doorway of the ChBD; ii) Further binding of GlcNAc units. However, binding through Ser33 remains inconclusive, since the mutational results revealed that Ser33 did not act as a powerful binding residue. Alternatively, this binding step might be made through a different surface-exposed aromatic residue located nearby; and iii) Sliding of bound sugar units of the chitin chain into the substrate binding cleft. Based on the 'slide and bend' mechanism proposed by Watanabe and others [17,21,32], the sliding process is achieved by cooperative interactions with other surface-exposed aromatic residues located close to the entrance of the substrate binding cleft. However, our data strongly suggested that the chitin chain movement most likely takes place via an interaction with different surface-exposed aromatic residues other than Tyr245 and Trp231.

When *p*NP-$[GlcNAc]_2$ was used as a substrate, hydrolyzing activities of the mutated enzymes and the wild-type enzyme were almost indistinguishable. This observation and the essentially unchanged catalytic efficiency (k_{cat}/K_m) of all mutants compared to wild-type enzyme clearly pointed out that Ser33, Trp70, Trp231 and Tyr245 do not play a major role in the process of hydrolysis of soluble chitooligosaccharides.

Conclusion

Point mutations of four surface-exposed residues of *V. carchariae* chitinase A and subsequent experiments on chitin binding and hydrolysis were performed. Trp70, which is located at the *N*-terminal end of the chitin binding domain, was identified as the most crucial residue in colloidal and crystalline chitin binding and consequently their hydrolysis. The residues Trp231 and Tyr245, both located nearer to the substrate-binding cleft, influenced chitin hydrolysis but not really insoluble chitin binding.

Methods

Bacterial strains and expression plasmid

Escherichia coli type strain DH5α was used for routine cloning, subcloning and plasmid preparation. Supercompetent *E. coli* XL1Blue (Stratagene, La Jolla, CA, USA) was the host strain for the production of mutagenized DNA.*E. coli* type strain M15 (Qiagen, Valencia, CA, USA) and the pQE 60 expression vector harboring *chitinase A* gene fragments were used for a high-level expression of recombinant chitinases.

A structural based sequence alignment and homology modeling

The amino acid sequence alignment was constructed by the program MegAlign using CLUSTAL method algorithm in the DNASTAR package (Biocompare, Inc., CA, USA) and displayed in Genedoc [33]. The amino acid sequence of the *V. carchariae* chitinase was aligned with five selected bacterial chitinase sequences available in the Swiss-Prot or TrEMBL database (see Results). The secondary structure elements of *V. carchariae* chitinase A were obtained by the PHD method available in PredicProtein [34]. The modeled tertiary structure of the *Vibrio* chitnase was built by Swiss-Model and displayed by Swiss-Pdb Viewer [35] using the x-ray structure of *S. marcescens* chitinase A E315L mutant complex with hexaNAG (PDB code: 1NH6) as structure template. The co-ordinates of $[GlcNAc]_6$ were modeled into the active site of the *Vibrio* enzyme and the target residues were located by superimposing the C_α atoms of 459 residues of *V. carchariae* chitinase A with the equivalent residues of *S. marcescens* E315L complex, using the program Superpose available in the CCP4 suit [36]. The predicted structure was viewed with Pymol [37].

Mutation design and site-directed mutagenesis

Site-directed mutagenesis was carried out by PCR using QuickChange site-directed mutagenesis kit (Stratagene). The pQE60 plasmid harbouring chitinase A DNA lacking the residues 598–850 *C*-terminal fragment was used as DNA template [25]. The primers (Bio Service Unit, Thailand) used for the mutagenesis are summarized in Table 3. The success of newly-generated mutations was confirmed by automated DNA sequencing (BSU, Thailand). The programs used for nucleotide sequence analyses were obtained from the DNASTAR package (DNASTAR, Inc., Madison, USA).

Expression and purification of recombinant wild-type and mutant chitinases

The pQE60 expression vector harboring the DNA fragment that encodes wild-type chitinase A were highly expressed in *E. coli* M15 cells and the recombinant proteins purified as described elsewhere [28]. Briefly, the cells were grown at 37°C in Luria Bertani (LB) medium containing 100 μg/ml ampicillin until OD_{600} reached 0.6, and then 0.5 mM of isopropyl thio-*β*-D-galactoside (IPTG) was added to the cell culture for chitinase production. After 18 h of induction at 25°C, the cell pellet was collected by centrifugation, re-suspended in 15 ml of lysis buffer (20 mM Tris-HCl buffer, pH 8.0, containing 150

Table 3: Primers used for mutagenesis

Point mutation	Oligonucleotide sequence
Ser33→Ala	Forward 5'-CGATATGTACGGTGCG[a]AATAACCTTCAATTTTC-3'
	Reverse 5'-GAAAATTGAAGGTTATTCGCACCGTACATATCG-3'
Ser33→Trp	Forward 5'-CGATATGTACGGTTGGAATAAC**CTG**[b]CAATTTTC-3'
	Reverse 5'-GAAAATTG**CAG**GTTATTCCAACCGTACATATCG-3'
Trp70→Ala	Forward 5'-GAAATTTAACCAGGCGAGTGGCACATCTG-3'
	Reverse 5'-CAGATGTGCCACTCGCCTGGTTAAATTTC-3'
Trp231→Ala	Forward 5'-GTTATCCAT**GAT**CCGGCGgcagcttatc-3'
	Reverse 5'-GATAAGCTGCCGCCGG**ATC**ATGGATAAC-3'
Trp231→Phe	Forward 5'-GGTTATCCATGACCCGTTTGCAGCTTATCAG-3'
	Reverse 5'-CTGATAAGCTGCAAACGGGTCATGGATAACC-3'
Tyr245→Trp	Forward 5'-CAGGTCATGAATGGAGCACGCCAATCAAG-3'
	Reverse 5'-CTTGATTGGCGTGCTCCATTCATGACCTG-3'

[a] Sequences underlined indicate the mutated codons.
[b] Sequences in bold represent the codon being modified to achieve the T_m value as required for QuickChange site-directed mutagenesis.

mM NaCl, 1 mM phenylmethylsulphonyl fluoride (PMSF), and 1.0 mg/ml lysozyme), and then lysed on ice using an Ultrasonic homogenizer. The supernatant obtained after centrifugation at 12,000 *g* for 1 h was instantly subjected to Ni-NTA agarose affinity chromatography following the Qiagen's protocol. After SDS-PAGE analysis [38], the chitinase containing fractions were pooled and then applied to Vivaspin-20 membrane filtration (*M*r 10 000 cut-off, Vivascience AG, Hannover, Germany) to concentrate the protein and to remove imidazole. A final concentration of the protein was determined by Bradford's method [39] using a standard calibration curve constructed from BSA (0–25 μg).

Chitinase activity assays

The colorimetric assay was carried out in a 96-well microtiter plate using *p*NP-$[GlcNAc]_2$ (Bioactive Co., Ltd., Bangkok, Thailand) as substrate. A 100-μl assay mixture, comprising protein sample (10 μl), 500 μM *p*NP-$(GlcNAc)_2$, and 100 mM sodium acetate buffer, pH 5.5, was incubated at 37°C for 10 min with shaking. After the reaction was terminated by the addition of 1.0 M Na_2CO_3 (50 μl), the amount of *p*-nitrophenol (*p*NP) released was determined by A_{405} in a microtiter plate reader (Applied Biosystems, Foster City, CA, USA). Molar concentrations of the *p*NP product were estimated from a calibration curve of *p*NP (0–30 nmol). Alternatively, chitinase activity was measured by a reducing-sugar assay. The reaction mixture (500 μl), containing 1% (w/v) colloidal chitin (prepared based on Hsu & Lockwood [40]), 100 mM sodium acetate buffer, pH 5.5, and 100 μg chitinase A, was incubated at 37°C in a Thermomixer comfort (Eppendorf AG, Hamburg, Germany). After 15 min of incubation, the reaction was terminated by boiling at 100°C for 5 min, and then centrifuged at 5,000 g for 10 min to precipitate the remaining chitin. A 200-μl supernatant was then subjected to DMAB assay following Bruce *et al.* [41]. The release of the reducing sugars as detected by A_{585} was converted to molar quantity using a standard calibration curve of $[GlcNAc]_2$ (0–1.75 μmol). For crystalline α-chitin, chitinase activity assay was carried out as described for colloidal chitin with 400 μg of chitinase A included in the assayed mixture.

Chitin binding assays

Chitin binding assays were carried out at 0°C to minimize hydrolysis. For time course studies, a reaction mixture (500 μl), containing 1.0 μmol enzyme, and 1.0 mg of chitin in 20 mM Tris-HCl buffer, pH 8.0, was incubated to a required time of 0, 1.25, 2.5, 5, 10, 15, 20, 25, and 30 min, and then the supernatant was collected by centrifuging at 12000 g at 4°C for 10 min. Concentration of the remaining enzyme was determined by Bradford's method, while concentration of the bound enzyme (E_b) was calculated from the difference between the initial protein concentration (E_t) and the free protein concentration (E_f) after binding.

The chitin binding assay was also carried out with crystalline chitin and colloidal chitin (Sigma-Aldrich Pte Ltd., The Capricorn, Singapore Science Park II, Singapore) as tested polysaccharides. A reaction (set as above) was incubated for 60 min at 0°C, then the chitin-bound enzyme was removed by centrifugation, and the concentration of the free enzyme was determined. For adsorption isotherm experiments, the reaction assay (also prepared as described above) containing varied concentrations of protein from 0 to 7.0 μM was incubated for 60 min. After centrifugation, concentration of free enzyme in the supernatant was determined. A plot of $[E_b]$ vs $[E_f]$ was subsequently constructed and the dissociation binding constants (K_d) of wild-type and mutants were estimated using

a non-linear regression function in the GraphPad Prism software (GraphPad Software Inc., San Diego, CA).

Steady-state kinetics

Kinetic parameters of the chitinase variants were determined using chitohexaose or colloidal chitin as substrate. For chitohexaose, the reaction mixture (200 μl), containing 0–500 μM $(GlcNAc)_6$, and 50 μg enzyme in 100 mM sodium acetate buffer, pH 5.5, was incubated at 37°C for 10 min. After boiling to 100°C for 3 min, the entire reaction mixture was subjected to DMAB assay as described earlier. For colloidal chitin, the reaction was carried out the same way as the reducing-sugar assay, but concentrations of colloidal chitin were varied from 0 to 5.0% (w/v). The amounts of the reaction products produced from both substrates were determined from a standard curve of $[GlcNAc]_2$ (0–1.75 μmol). The kinetic values were evaluated from three independent sets of data using the nonlinear regression function obtained from the GraphPad Prism software.

Abbreviations

$GlcNAc_n$: β-1–4 linked oligomers of *N*-acetylglucosamine residues where n = 1–6; DMAB: *p*-dimethylaminobenzaldehyde; IPTG: Isopropyl thio-β-D-galactoside; PMSF: Phenylmethylsulphonylfluoride.

Authors' contributions

SP performed site-directed mutagenesis, recombinant expression, protein purification, and functional characterization. CS carried out the sturcture-based sequence alignment and the molecular modeling of the tertiary structure of V. carchariae chitinase A. WS initiated the ideas of research, was involved in primer design and site-directed mutagenesis, performed data analyses, and prepared the manuscript.

Acknowledgements

This work was financially supported by Suranaree University of Technology; The Thailand Research Fund (TRF) and The Thai Commission on Higher Education through a Research Career Development Grant to WS (grant no RMU4980028) and a TRF-Master Research Grant to SP (grant no MRG495S044).

References

1. Yu C, Lee AM, Bassler BL, Roseman S: **Chitin utilization by marine bacteria. A physiological function for bacterial adhesion to immobilized carbohydrates.** *J Biol Chem* 1991, **266:**24260-24267.
2. Rast DM, Horsch M, Furter R, Gooday GW: **A complex chitinolytic system in exponentially growing mycelium of *Mucor rouxii*: properties and function.** *J Gen Microbiol* 1991, **137:**2797-2810.
3. Merzendorfer H, Zimoch L: **Chitin metabolism in insects:structure, function and regulation of chitin synthases and chitinases.** *J Exp Biol* 2003, **206:**4393-4412.
4. Herrera-Estrella A, Chet I: **Chitinases in biological control.** *EXS* 1999, **87:**171-184.
5. Melchers LS, Stuiver MH: **Novel genes for disease-resistance breeding.** *Curr Opin Plant Biol* 2000, **3:**147-152.
6. Patil RS, Ghormade VV, Deshpande MV: **Chitinolytic enzymes: an exploration.** *Enzyme Microb Technol* 2000, **26:**473-483.
7. Donnelly LE, Barnes PJ: **Acidic mammalian chitinase – a potential target for asthma therapy.** *TRENDS in Pharmacol Sci* 2004, **25:**509-511.
8. Wills-Karp M, Karp CL: **Chitin checking-novel insights into asthma.** *N Engl J Med* 2004, **351:**1455-1457.
9. Terwisscha van Scheltinga AC, Kalk KH, Beintema JJ, Dijkstra BW: **Crystal structures of hevamine, a plant defence protein with chitinase and lysozyme activity, and its complex with an inhibitor.** *Structure* 1994, **15:**1181-1189.
10. Perrakis A, Tews I, Dauter Z, Oppenheim AB, Chet I, Wilson KS, Vorgias CE: **Crystal structure of a bacterial chitinase at 2.3 Å resolution.** *Structure* 1994, **15:**1169-1180.
11. Hart PJ, Pfluger HD, Monzingo AF, Hollis T, Robertus JD: **The refined crystal structure of an endochitinase from *Hordeum vulgare* L. seeds at 1.8 Å resolution.** *J Mol Biol* 1995, **248:**402-413.
12. Watanabe T, Oyanagi W, Suzuki K, Tanaka H: **Chitinase system of *Bacillus circulans* WL-12 and importance of chitinase A1 in chitin degradation.** *J Bacteriol* 1990, **172:**4017-4022.
13. Suzuki K, Sugawara N, Suzuki M, Uchiyama T, Katouno F, Nikaidou N, Watanabe T: **Chitinases A, B, and C1 of *Serratia marcescens* 2170 produced by recombinant *Escherichia coli*: enzymatic properties and synergism on chitin degradation.** *Biosci Biotechnol Biochem* 2002, **66:**1075-1083.
14. Montgomery MT, Kirchman DL: **Role of chitin-binding proteins in the specific attachment of the marine bacterium *Vibrio harveyi* to chitin.** *Appl Environ Microbiol* 1993, **59:**373-379.
15. Tsujibo H, Orikoshi H, Baba N, Miyahara M, Miyamoto K, Yasuda M, Inamori Y: **Identification and characterization of the gene cluster involved in chitin degradation in a marine bacterium, *Alteromonas* sp. strain O-7.** *Appl Environ Microbiol* 2002, **68:**263-270.
16. Suginta W: **Identification of chitin binding proteins and characterization of two chitinase isoforms from *Vibrio alginolyticus* 283.** *Enzyme Microb Tech* 2007, **41:**212-220.
17. Watanabe T, Ishibashi A, Ariga Y, Hashimoto M, Nikaidou N, Sugiyama J, Matsumoto T, Nonaka T: **Trp122 and Trp134 on the surface of the catalytic domain are essential for crystalline chitin hydrolysis by *Bacillus circulans* chitinase A1.** *FEBS Lett* 2001, **494:**74-78.
18. Uchiyama T, Katouno F, Nikaidou N, Nonaka T, Sugiyama J, Watanabe T: **Roles of the exposed aromatic residues in crystalline chitin hydrolysis by chitinase A from *Serratia marcescens* 2170.** *J Biol Chem* 2001, **276:**41343-41349.
19. Katouno F, Taguchi M, Sakurai K, Uchiyama T, Nikaidou N, Nonaka T, Sugiyama J, Watanabe T: **Importance of exposed aromatic residues in chitinase B from *Serratia marcescens* 2170 for crystalline chitin hydrolysis.** *J Biochem (Tokyo)* 2004, **136:**163-168.
20. Itoh Y, Watanabe J, Fukada H, Mizuno R, Kezuka Y, Nonaka T, Watanabe T: **Importance of Trp59 and Trp60 in chitin-binding, hydrolytic, and antifungal activities of *Streptomyces griseus* chitinase C.** *Appl Microbiol Biotechnol* 2006, **72:**1176-1184.
21. Imai T, Watanabe T, Yui T, Sugiyama J: **Directional degradation of beta-chitin by chitinase A1 revealed by a novel reducing end labelling technique.** *FEBS Lett* 2002, **510:**201-205.
22. Hult EL, Katouno F, Uchiyama T, Watanabe T, Sugiyama J: **Molecular directionality in crystalline beta-chitin: hydrolysis by chitinases A and B from *Serratia marcescens* 2170.** *Biochem J* 2005, **388:**851-856.
23. Li Q, Wang F, Zhou Y, Xiao X: **Putative exposed aromatic and hydroxyl residues on the surface of the *N*-terminal domains of Chi1 from *Aeromonas caviae* CB101 are essential for chitin binding and hydrolysis.** *Appl Environ Microbiol* 2005, **71:**7559-7561.
24. Suginta W, Robertson PAW, Austin B, Fry SC, Fothergill-Gilmore LA: **Chitinases from *Vibrio*: activity screening and purification of Chi A from *Vibrio carchariae*.** *J Appl Microbiol* 2000, **89:**76-84.
25. Suginta W, Vongsuwan A, Songsiriritthigul C, Prinz H, Estibeiro P, Duncan RR, Svasti J, Fothergill-Gilmore LA: **An endochitinase A from *Vibrio carchariae*: cloning, expression, mass and sequence analyses, and chitin hydrolysis.** *Arch Biochem Biophys* 2004, **424:**171-180.
26. Suginta W, Vongsuwan A, Songsiriritthigul C, Svasti J, Prinz H: **Enzymatic properties of wild-type and active site mutants of chi-**

tinase A from *Vibrio carchariae*, as revealed by HPLC-MS. *FEBS J* 2005, **272:**3376-386.
27. Tews I, Terwisscha van Scheltinga AC, Perrakis A, Wilson KS, Dijkstra BW: **Substrate-assisted catalysis unifies two families of chitinolytic enzymes.** *J Am Chem Soc* 1997, **119:**7954-7959.
28. Suginta W, Songsiriritthigul C, Kobdaj A, Opassiri R, Svasti J: **Mutations of Trp275 and Trp397 altered the binding selectivity of *Vibrio carchariae* chitinase A.** *Biochim Biophys Acta* 2007, **1770:**1151-1160.
29. Watanabe T, Ito Y, Yamada T, Hashimoto M, Sekine S, Tanaka H: **The roles of the C-terminal domain and type III domains of chitinase A1 from *Bacillus circulans* WL-12 in chitin degradation.** *J Bacteriol* 1994, **176:**4465-4472.
30. Ikegami T, Okada T, Hashimoto M, Seino S, Watanabe T, Shirakawa M: **Solution Structure of the chitin-binding domain of *Bacillus circulans* WL-12 chitinase A1.** *J Biol Chem* 2000, **275:**13654-13661.
31. Li Y, Irwin DC, Wilson DB: **Processivity, substrate binding, and mechanism of cellulose hydrolysis by *Thermobifida fusca* Cel9A.** *Appl Environ Microbiol* 2007, **73:**3165-3172.
32. Watanabe T, Ariga Y, Sato U, Toratani T, Hashimoto M, Nikaidou N, Kezuka Y, Nonaka T, Sugiyama J: **Aromatic residues within the substrate-binding cleft of *Bacillus circulans* chitinase A1 are essential for hydrolysis of crystalline chitin.** *Biochem J* 2003, **376:**237-244.
33. **The National Resource for Biomedical Supercomputing (NRBSC)** [http://www.psc.edu/biomed/genedoc/]
34. **PredictProtein** [http://www.predictprotein.org/]
35. **Swiss-Model** [http://swissmodel.expasy.org/]
36. Collaborative Computational Project, No.4: **The CCP4 suite: programs for protein crystallography.** *Acta Crystallogr* 1994, **D50:**760-763.
37. **PyMol** [http://www.pymol.org/]
38. Laemmli UK: **Cleavage of structural proteins during the assembly of the head of bacteriophage T4.** *Nature* 1970, **227:**680-685.
39. Bradford MM: **A rapid and sensitive method for the quantitation of microgram quantities of protein utilizing the principle of protein-dye binding.** *Anal Biochem* 1976, **72:**248-254.
40. Hsu SC, Lockwood JL: **Powdered chitin agar as a selective medium for enumeration of actinomycetes in water and soil.** *Appl Microbiol* 1975, **29:**422-426.
41. Bruce A, Srinivasan U, Staines HJ, Highley TL: **Chitinase and laminarinase production in liquid culture by *Trichoderma* spp. and their role in biocontrol of wood decay fungi.** *Int Biodeterior Biodegrad* 1995, **35:**337-353.

Journal of Structural Biology 162 (2008) 491–499

Contents lists available at ScienceDirect

Journal of Structural Biology

journal homepage: www.elsevier.com/locate/yjsbi

Crystal structures of *Vibrio harveyi* chitinase A complexed with chitooligosaccharides: Implications for the catalytic mechanism

Chomphunuch Songsiriritthigul [a,b], Supansa Pantoom [a], Adeleke H. Aguda [c,d], Robert C. Robinson [c], Wipa Suginta [a,*]

[a] School of Biochemistry, Suranaree University of Technology, Nakhon Ratchasima 30000, Thailand
[b] National Synchrotron Research Center, Nakhon Ratchasima 30000, Thailand
[c] Institute of Molecular and Cell Biology, Proteos, 61 Biopolis Drive, Singapore 138673, Singapore
[d] Department of Biology, University of Virginia, Charlottesville, VA 22904, USA

ARTICLE INFO

Article history:
Received 13 December 2007
Received in revised form 14 March 2008
Accepted 18 March 2008
Available online 26 March 2008

Keywords:
Chitinase
Chitin oligosaccharide
Crystal structure
The slide-and-bend mechanism
Vibrio harveyi

ABSTRACT

This research describes four X-ray structures of *Vibrio harveyi* chitinase A and its catalytically inactive mutant (E315M) in the presence and absence of substrates. The overall structure of chitinase A is that of a typical family-18 glycosyl hydrolase comprising three distinct domains: (i) the amino-terminal chitin-binding domain; (ii) the main catalytic $(\alpha/\beta)_8$ TIM-barrel domain; and (iii) the small $(\alpha+\beta)$ insertion domain. The catalytic cleft of chitinase A has a long, deep groove, which contains six chitooligosaccharide ring-binding subsites $(-4)(-3)(-2)(-1)(+1)(+2)$. The binding cleft of the ligand-free E315M is partially blocked by the *C*-terminal $(His)_6$-tag. Structures of E315M-chitooligosaccharide complexes display a linear conformation of pentaNAG, but a bent conformation of hexaNAG. Analysis of the final $2F_o - F_c$ omit map of E315M-NAG6 reveals the existence of the linear conformation of the hexaNAG at a lower occupancy with respect to the bent conformation. These crystallographic data provide evidence that the interacting sugars undergo conformational changes prior to hydrolysis by the wild-type enzyme.

1. Introduction

Chitin, a highly stable homopolysaccharide of β (1 → 4)-linked *N*-acetyl-D-glucosamine (GlcNAc or NAG)[1] is widely distributed in the shells of crustaceans; the cuticles of insects; the shells and skeletons of molluscs; and the cell walls of fungi. Chitin degradation is of considerable interest because the products have potential applications in the fields of biomedicine, agriculture, nutrition, and biotechnology. Chitinases (EC 3.2.1.14) are major enzymes that hydrolyse chitin into oligosaccharide fragments. These enzymes are found in organisms that possess chitin as a constituent or that use it as a nutrient source. Bacteria produce chitinases in order to utilise chitin as a source of carbon and nitrogen (Bhattacharya et al., 2007; Keyhani and Roseman, 1999). Fungal chitinases play a similar nutritional role but are additionally involved in fungal development and morphogenesis (Kuranda and Robbins, 1991; Sahai and Manocha, 1993). Plants produce chitinases as a defence mechanism against pathogenic fungi (Leah et al., 1991). Animal chitinases are involved in dietary uptake processes (Jeuniaux, 1961). Human chitinases are responsible for hyperresponsiveness and inflammation of the airways of allergic asthma patients (Donnelly and Barnes, 2004; Kawada et al., 2007).

The carbohydrate active enzyme (CAZy) database (http://www.cazy.org/) classifies carbohydrate enzymes into functional families (glycosyl hydrolases, glycosyl transferases, polysaccharide lyases, carbohydrate esterases, and carbohydrate-binding modules), which are further subdivided into structurally related families designated by number. Following this classification, chitinases are listed as GH family-18 and GH family-19. These two families show no homology in both structure and mechanism. The catalytic domain of family-18 chitinases consists of an $(\alpha/\beta)_8$-barrel with a deep substrate-binding cleft formed by loops following the C-termini of the eight parallel β-strands (Fukamizo, 2000; Hollis et al., 2000; Perrakis et al., 1994; Terwisscha van Scheltinga et al., 1996). In contrast, the catalytic domain of family-19 chitinases comprises two lobes, each of which is rich in α-helical structure (Hart et al., 1995). Family-18 chitinases are known to catalyse the hydrolytic reaction through the 'substrate-assisted' or'retaining mechanism' (Brameld and Goddard, 1998a; Terwisscha van Scheltinga et al., 1995; Tews et al., 1997), whereas family 19 chitinases employ the 'single displacement' or 'inversion mechanism' (Brameld and Goddard, 1998b). The catalytic mechanism of family-18 chitinases involves protonation of the leaving

* Corresponding author. Fax: +66 44 224185.
E-mail address: wipa@sut.ac.th (W. Suginta).

[1] *Abbreviations used:* GlcNAc or NAGn, β-1-4 linked oligomers of *N*-acetylglucosamine residues where *n* = 1–6; *p*NP-$[GlcNAc]_2$, *p*-nitrophynyl-β-D-*N,N'*-diacetylchitobioside; IPTG, isopropyl thio-β-D-galactoside; PMSF, phenylmethylsulphonylfluoride; ChBD, the amino-terminal chitin-binding domain.

1047-8477/$ - see front matter © 2008 Elsevier Inc. All rights reserved.
doi:10.1016/j.jsb.2008.03.008

group by an absolutely conserved glutamic acid (equivalent to Glu315 of *Serratia marcescens* chitinase A), followed by substrate distortion into a 'boat' conformation at subsite −1 and the stabilisation of an oxazolinium intermediate by the sugar *N*-acetamido group. The resultant bond cleavage yields the retention of anomeric configuration in the products (Armand et al., 1994; Fukamizo et al., 2001; Honda et al., 2004; Sasaki et al., 2002).

Chitinases from both families are further divided into exo- and endochitinases. Exochitinase activity represents a progressive action that starts at the non-reducing end of a chitin chain and successively releases diacetylchitobiose (NAG2) units, where as, endochitinase activity involves random cleavage at internal points within a chitin chain (Robbins et al., 1988). The active sites of family-18 endochitinases, such as *S. marcescens* chitinase A and *Hevea brasiliensis* chitinase (hevamine), are groove-like structures with openings above and at both ends (Brameld and Goddard, 1998a; Hart et al., 1995). In contrast, the active sites of exochitinases, such as *S. marcescens* ChiB, have tunnel-like morphologies (Van Aalten et al., 2001).

We previously isolated the Chi A gene encoding the 95-kDa chitinase precursor (GenBank Accession No: Q9AMP1) from the genome of *Vibrio carchariae* type strain LMG7890. Based on genotypical and phenotypical features analysed by Pedersen et al. (1998), *V. carchariae* has been re-classified as a heterotypic synonym of *Vibrio harveyi*. To follow the new systematic taxonomy, *V. carchariae* will be referred to as *V. harveyi* in this and later studies. *V. harveyi* (formerly *V. carchariae*) is a marine bacterium that secretes high levels of a 63-kDa endochitinase A (Suginta et al., 2000). This family-18 glycosyl hydrolase shows greatest affinity towards chitohexamer, which suggests the substrate-binding cleft of this enzyme that comprises an array of six GlcNAc-binding sites (Suginta et al., 2005), comparable to that of *S. marcescens* Chi A and hevamine (Papanikolau et al., 2001; Perrakis et al., 1994; Terwisscha van Scheltinga et al., 1996). The gene that encodes chitinase A without the 253-aa *C*-terminal proprotein fragment was subsequently cloned and functionally expressed in *Escherichia coli* (Suginta et al., 2004). Substitution of Glu315 to Met/Gln completely abolished the hydrolysing activity against soluble and insoluble substrates, confirming that this residue is essential for catalysis (Suginta et al., 2005).

In this study, we describe the crystal structures of *V. harveyi* chitinase A and its catalytically inactive E315M mutant, as well as the E315M mutant soaked with NAG5 and NAG6. The overall structures of E315M with and without substrates are almost identical to the wild-type structure. However, the relative conformations of NAG5 and NAG6 bound to E315M are very different. These static structures provide hints to the conformational changes in chitooligosaccharide conformation during binding and hydrolysis, allowing for a catalytic mechanism of the enzyme to be proposed.

2. Experimental procedures

2.1. Cloning, recombinant expression, and purification

Wild-type chitinase A (amino-acid residues 22–597) and mutant E315M were cloned into the *C*-terminal $(His)_6$ tag pQE60 expression vector, and were highly expressed in *E. coli* type strain M15 (Suginta et al., 2004). For protein purification, IPTG-induced bacterial cells obtained from 1-L culture were collected by centrifugation and then resuspended in 20 ml of 20 mM Tris–HCl (pH 8.0) containing 150 mM NaCl, 1 mg ml^{-1} lysozyme, and 1 tablet of cØmplete EDTA-free, Protease Inhibitor Cocktail (Roche Diagnostics GmbH, Roche Applied Science, Germany). The cells were lysed on ice using a Misonix Sonicator 3000 (New Highway Farmingdale, NY, USA) with a 20-mm-diameter probe. After the removal of cell debris by centrifugation, the supernatant was filtered through a SFCA membrane (0.2 μm pore size, Nalgene, Rochester, NY, USA) prior to application to two HisTrap HP 1-ml columns connected in series using an ÄKTAxpress purification system (Amersham Biosciences, Piscataway, NJ, USA.) and a flow rate of 2.8 ml min^{-1}. The columns were washed with 5 mM, followed by 20 mM, imidazole before being eluted with 250 mM imidazole in 20 mM Tris–HCl (pH 8.0), containing 150 mM NaCl. The protein-containing fractions were collected, concentrated using Vivaspin-20 membrane concentrator (Mr 10,000 cut-off, Vivascience AG, Hannover, Germany), and then further purified by an ÄKTAxpress system using a HiLoad 16/60 Superdex 200 prep grade (Amersham Biosciences) with a flow rate of 1.2 ml min^{-1}. Chitinase-containing fractions were combined, exchanged into 10 mM Tris–HCl (pH 8.0), and concentrated to 10–20 mg ml^{-1} using the Vivaspin membrane concentrator. All purification steps were carried out at 277 K. Protein concentrations were determined by the Coomassie Plus Kit (Pierce, Rockford, IL, USA) using a standard calibration curve constructed from BSA (0–20 μg). The purity of chitinase A was verified by SDS–PAGE (Laemmli, 1970). Chitinase activity was determined by colorimetric assay using *p*NP-$[GlcNAc]_2$ as substrate (Suginta et al., 2007) or by the reducing sugar assay using colloidal chitin as substrate (Bruce et al., 1995).

2.2. Protein crystallisation

Initial crystallisation trials of the wild-type chitinase A were set up using a Screenmaker 96+8™ Robot (Innovadyne Technologies, Inc., Santa Rosa, CA, USA) with sitting drop CrystalQuick™ plates (Greiner bio-one, Frickenhausen, Germany). For each crystallisation drop, 20 nl of freshly prepared enzyme (20 mg ml^{-1}) in 10 mM Tris–HCl (pH 8.0), was added to 20 nl of each precipitating agent obtained commercially (Crystal Screen HT & SaltRx HT from Hampton Research, Aliso Viejo, CA, USA, and JBScreen HTS I & II from Jena Bioscience GmbH, Jena, Germany). Crystal growth optimisation with macro seeding was carried out under several JBScreen HTS II precipitant conditions. Diffraction quality crystals, dimensions 230 × 100 × 15 μm^3, were produced within two days at 288 K when a protein drop (5 mg ml^{-1}) was equilibrated in 1.2 M ammonium sulphate and 0.1 M Tris–HCl (pH 8.0). The E315M crystals were obtained from 20% (w/v) PEG 4000, 0.1 M ammonium sulphate and 0.1 M Tris–HCl (pH 7.5) and reached final dimensions of 100 × 30 × 50 μm^3 after 1 week equilibration at 288 K. Prior to soaking experiments, single crystals of E315M grown under 16% (w/v) PEG 4000, 0.1 M $MgCl_2$ in 0.1 M HEPES (pH 7.0.) were transferred to a cryoprotectant solution containing mother liquor with 20% (w/v) PEG 4000, and 10% (v/v) glycerol and 10 mM NAG5 or NAG6. The crystals were then soaked overnight at 288 K before being mounted directly into a nitrogen cryostream for data collection.

2.3. Data collection, processing, and structure determination

All the X-ray diffraction data were collected by a Rikagu/MSC FR-E Super Bright equipped with an R-AXIS IV++ imaging plate detector. Data processing was conducted with the program MOSFLM (Leslie, 1991) and molecular replacement was employed to obtain phase information using the program AmoRe from the CCP4 suite (Navaza, 1994). The E315M data set was solved using the crystal structure of *S. marcescens* chitinase A (PDB code 1CTN; 47% identical to *V. harveyi* chitinase A) as a search model. Alternate sessions of model rebuilding in O (Jones et al., 1991) and restrained refinement in REFMAC from the CCP4 suite (Collaborative Computational Project Number 4, 1994; Murshudov et al.,

1997) were continued until the values of the free *R*-factor converged. Crystallographic data and refinement statistics of the chitinase structures are summarised in Table 1.

The final model of E315M was employed as the model for the subsequent three data sets of E315M+NAG5, E315M+NAG6, and the wild-type enzyme. Sugar coordinates taken from the protein databank (PDB code 1NH6) were modelled into the $2F_o - F_c$ and $F_o - F_c$ maps, and further refined. During the model rebuilding process, the non-reducing end unit of NAG5 (−4NAG) showed poor electron density. Examination of the refined structure of E315M+NAG6 exhibited ambiguity in the electron density of the +1 NAG and −1NAG in the $2F_o - F_c$ omit map showing partial density for the NAG5 conformation. The final free *R*-factors from modelling NAG6, NAG5, or no ligand into the E315M+NAG6 data are 21.0%, 21.4%, and 21.7%, respectively.

Tight non-crystallographic symmetry restraints were initially employed in refining the wild-type structure but later released as judged by the free *R*-factor. The geometry of each final model was verified by PROCHECK (Laskowski et al., 1993). No residues lie in the disallowed regions of the Ramachandran plots. Three residues (590, 591, and 592) could not be modelled into the E315M structures due to their poor electron density. The C-terminal hexahistidine tag was clear in the electron density of the ligand-free E315M but absent from the other structures. The refined structures of the four enzyme forms were compared within the program Superpose and direct contacts determined in the program Contact (CCP4 suite). The structures and electron density maps were created and displayed by Pymol (www.pymol.org).

2.4. Fluorescence studies of chitooligosaccharide binding

The interactions of NAG5 and NAG6 with E315M/Q were studied by fluorescence spectroscopy. The purified proteins (0.25 μM) were titrated with ligand (0.01–20 μM) in 20 mM Tris–HCl (pH 8.0) and changes in the intrinsic tryptophan fluorescence (Srivastava et al., 2006) were directly monitored on an LS-50 fluorescence spectrometer (Perkin-Elmer Limited (Instruments & Life Sciences), Bangkok, Thailand). The measurements were conducted at 25 °C with an excitation wavelength of 295 nm and emission intensities collected over 300–450 nm. The excitation and emission slit widths were kept at 5 nm. Each protein spectrum was corrected for the buffer spectrum. The fluorescence intensity data were analysed by non-linear regression function available in GraphPad Prism version 3.0 (GraphPad Software, California, USA) using the following single-site-binding equation: where $F - F_0 = \frac{(F_b - F_0)\times(L_0)}{K_d + (L_0)} F$ and F_0 refer to the fluorescence intensity in the presence and absence of ligand, respectively; F_b refers to the maximum fluorescence signal of the protein-ligand complex; L_0 is the initial ligand concentration and K_d is the equilibrium dissociation constant.

3. Results and discussion

3.1. The overall structures of V. harveyi chitinase A

The overall structures of the native chitinase A, mutant E315M with and without substrates are essentially identical and closely

Table 1
Statistics of data and structural refinement

Crystal	Wild-type	E315M	E315M+NAG_5	E315M+NAG_6
Data collection statistics				
PDB code	3B8S	3B9E	3B9D	3B9A
Space group	*P*1	$P2_12_12_1$	$P2_12_12_1$	$P2_12_12_1$
Unit-cell parameters	*a* = 60.27 Å b = 64.28 Å c = 83.52 Å α = 91.74° β = 91.18° γ = 112.91°	*a* = 63.96 Å b = 83.11 Å c = 106.98 Å α = β = γ = 90°	*a* = 63.51 Å b = 83.08 Å c = 105.59 Å α = β = γ = 90°	*a* = 63.70 Å b = 83.32 Å C = 106.57 Å α = β = γ = 90°
Resolution range[a] (Å)	24.62–2.11 (2.00)	24.68–1.79 (1.70)	24.54–1.81 (1.72)	30–1.90 (1.80)
Solvent content (%)	46.9	44.85	43.70	44.55
Unique reflections	73693 (10404)	61563 (7880)	59561(8247)	53131 (7564)
Observed reflections	292719 (41321)	607216 (59894)	406849 (45783)	452556 (63380)
Multiplicity	4.0 (4.0)	9.9 (7.6)	6.8 (5.6)	8.5 (8.4)
Completeness (%)	94.6 (91.9)	97.2 (87.2)	99.2 (95.6)	99.7 (99.0)
⟨*I*/sigma*I*⟩	19.5 (5.5)	26.9 (4.5)	26.3 (9.9)	26.3 (6.1)
R_{merge}[a,b] (%)	6.6 (22.8)	7.1 (36.1)	7.1 (12.3)	7.0 (31.2)
Refinement statistics				
R_{factor}[c](%)	16.8	18.9	18.7	18.1
R_{free}[d](%)	20.5	21.9	21.5	21.0
No. of amino acid residues	1134	581	567	567
No. of protein atoms	8708	4474	4353	4353
No. of carbohydrate atoms	–	–	57	85
No. of ordered waters	1091	740	664	690
R.M.S. deviations				
Bond length	0.007	0.006	0.006	0.006
Bond angle	0.968	0.932	0.962	0.990
Mean atomic				
B values Protein atoms	14.45	15.10	14.24	13.74
Substrate	–	–	19.82	21.79
Waters	24.46	25.69	24.92	25.42
Overall	16.19	16.60	15.70	15.45

[a] Values in parentheses refer to the corresponding values of the highest resolution shell.

[b] $R_{merge} = \sum_{hkl}\sum_i |Ii(hkl) - \langle I(hkl)\rangle| / \sum_{hkl}\sum_i Ii(hkl)$ where I_i is the intensity for the *i*th measurement of an equivalent reflection with indices *hkl*.

[c] $R_{factor} = \frac{\sum ||F_{obs}| - |F_{calc}||}{\sum |F_{obs}|}$ where F_{obs} and F_{calc} are the observed and calculated structure-factors.

[d] $R_{free} = \frac{\sum ||F_{obs}| - |F_{calc}||}{\sum |F_{obs}|}$ calculated from 5% of the reflections selected randomly and omitted from the refinement process.

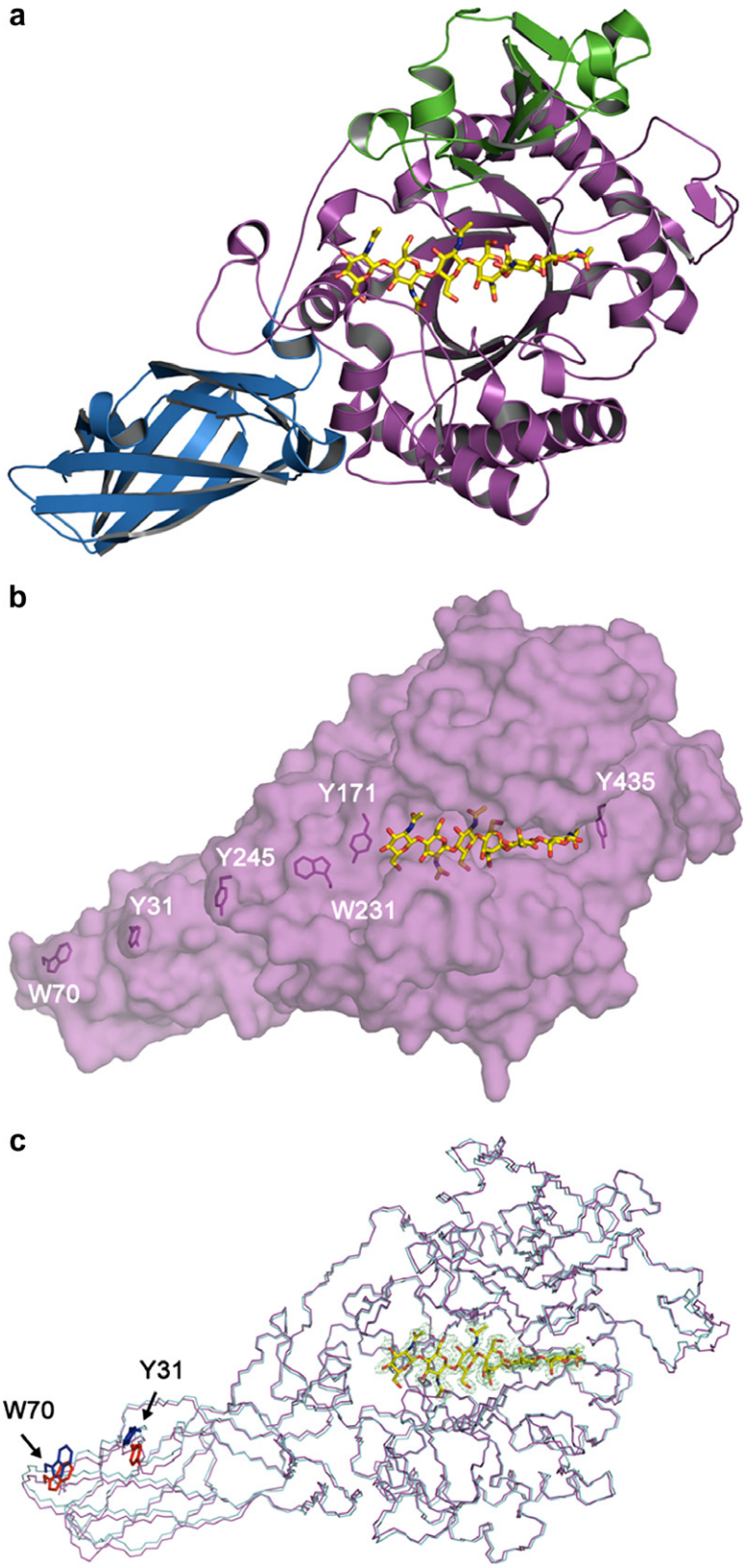

Fig. 1. The overall structure of *V. harveyi* chitinase A (a) The structure of catalytically inactive mutant E315M complexed with NAG_6. The *N*-terminal ChBD domain is in blue, the catalytic TIM-barrel domain in magenta, and the small insertion domain in green. (b) Surface representation of E315M showing the positions of the regularly spaced, surface-exposed hydrophobic residues. Y435 marks the reducing end of NAG6 and Y171 marks the non-reducing end. The linear track of hydrophobic residues extending away from the non-reducing end of NAG6 suggests the binding path for longer chain chitins. (c) A superimposition of wild-type chitinase A with E315M+NAG6. The backbone structure of the wild-type is depicted in cyan and of E315M+NAG_6in magenta. The residues Trp70 and Tyr31 located at the end of the ChBD and other aromatic residues located at the exterior of the TIM barrel domain (Y245, Trp231, Tyr171) and Tyr435 that marks the reducing end of the catalytic cleft are shown in blue for wild-type and red for E315M+NAG_6. Sugar units are shown as $2F_o - F_c$ map and sticks (yellow).

resemble those of chitinase A from *S. marcescens* and chitinase-1 from the pathogenic fungus *Coccidioides immitis* with minor dissimilarities in loop and helical regions (Perrakis et al., 1994; Hollis et al., 2000). Fig. 1a represents the structure of the chitinase A E315M mutant, which comprises three distinct domains, bound to hexaNAG. The amino-terminal chitin-binding domain (ChBD, blue) has a β-strand-rich fold formed by residues 22–138. This domain is connected to the core domain by a 21 amino-acid linker peptide (residues 139–159). The catalytic domain (magenta) has a $(\alpha/\beta)_8$-TIM barrel fold consisting of eight β-strands (B1–B8) tethered to eight α-helices (A1–A8) by loops and is made up of two parts, referred to as Cat I (residues 160–460) and Cat II (residues 548–588). The catalytic residue (Glu315) is positioned in the loop of strand B4, which is part of a DxxDxDxE conserved motif. The α + β-fold insertion domain (green) connects strand B7 of Cat I and helix A7 of Cat II and is made up of five anti-parallel β-strands flanked by short α-helices (residues 461–547). This small domain provides a signature for subfamily A chitinases (Suzuki et al., 1999), although its function remains to be identified. As observed in this study, a few residues from this domain contribute to binding both NAG5 and NAG6 (Fig. 2).

The four structures exhibit three notable common structural features: (i) Tyr171 is detected in a generously allowed region in the Ramachandran plot and lines in the substrate-binding pocket; (ii) three cis peptide bonds are formed between the residues Gly191–Phe192, Glu315–Phe316, and Trp570–Glu571, all located at the exterior of the catalytic cleft; and (iii) three internal disulfide bonds are observed, one of which (Cys116–Cys121) is found at the end of the ChBD, and two others (Cys196–Cys217 & Cys409–Cys418) are present on the surface of the substrate-binding cleft. The existence of the conserved non-proline cis peptide bonds in the structures of *S. marcescens* chitinase A, *C. immitis* chitinase-1 and hevamine has been proposed to achieve essential conformational constraints (Hollis et al., 2000; Perrakis et al., 1994; Terwisscha van Scheltinga et al., 1996). The three non-proline cis peptide bonds, the two Cys196–Cys217 and Cys409–Cys418 disulfide bonds and residue Tyr171 define a general outline of the active site of the *Vibrio* chitinase (data not shown).

As in other family-18 chitinase 3D-structures (Fusetti et al., 2002; Hollis et al., 2000; Matsumoto et al., 1999; Perrakis et al., 1994; Terwisscha van Scheltinga et al., 1994; Van Aalten et al., 2000), the catalytic domain of *V. harveyi* chitinase A is an $(\alpha/\beta)_8$-TIM barrel fold. The structure of E315M+NAG6 complex reveals the substrate-binding cleft as a long, deep groove with estimated dimensions of 33 Å (long) × 14 Å (deep) × 13 Å (wide), which contains six-binding subsites (−4)(−3)(−2)(−1)(+1)(+2), Fig. 1b and 2c. This subsite topology defines subsite −4 at the non-reducing end (NRE), subsite +2 at the reducing end (RE) and the cleavage site between −1 and +1 sites. Similar subsites have been identified for *S. marcescens* chitinase A (Aronson et al., 2003; Papanikolau et al., 2001). In contrast, NAG5 occupies only four subsites (−3)(−2)(+1)(+2) of the binding cleft of E315M (Fig. 2a).

Four aromatic residues (Tyr31 & Trp70 from ChBD and Trp231 & Tyr245 at the edge of the non-reducing end of the substrate-binding sites) appear to line up in positions suitable for binding to longer chain chitins (Fig. 1b). Point mutations of these surface-exposed residues to Gly or Ala resulted in a notable decrease in the binding activity of *S. marcescens* Chi A, *B. circulans* Chi A1, and *Aeromnas caviae* Chi1 towards crystalline chitin (Li et al., 2005; Watanabe et al., 2001; Uchiyama et al., 2001). Our recent report further confirmed that Trp70 acts as the most crucial-binding residue for insoluble chitin, but had no effect on soluble chitooligosaccharides (Pantoom et al., 2008).

Superimposition of the four structures gives R.M.S. deviations in C^{α} positions of 0.63–0.77 Å for the 567 residues. Variation in the wild-type and the E315M+NAG6 structures is apparent as a slight variation in the angle between the ChBD and the catalytic domain (Fig. 1c). The catalytic domains of the two structures superimpose well but leave their ChBDs offset, resulting in a relative displacement of C^{α}-Trp70 (the critical chitin-binding residue) of 1.46 Å and the C^{α}-Tyr31 of 2.03 Å. This tilt suggests some innate flexibility between the two domains and may be involved in the sliding mechanism (as proposed by Watanabe et al., 2003) of a chi-

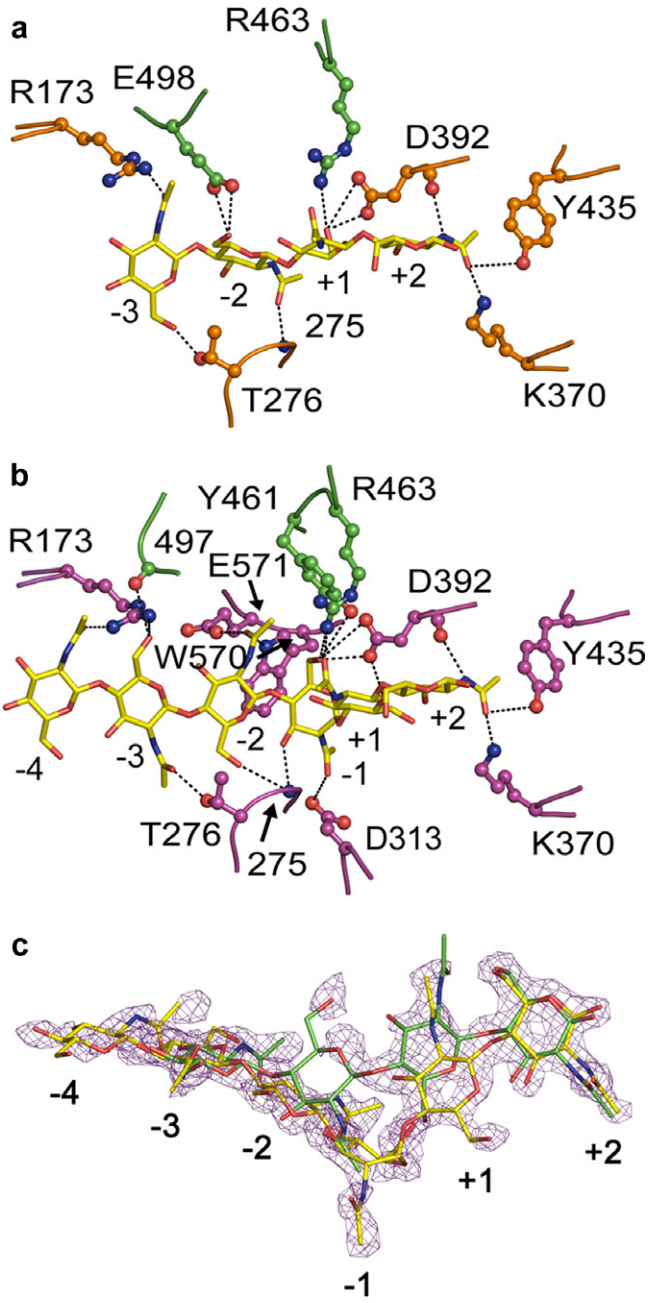

Fig. 2. Specific interactions within the substrate-binding cleft of E315M Interactions of (a) NAG_5 and (b) NAG_6. Hydrogen bonds are shown as dashed lines (. . ..). The binding residues are depicted as ball-and-stick with the sugar residues in a stick model. Carbon atoms of the binding residues in the catalytic domain are coloured orange for NAG_5 and magenta in NAG_6. Green represents carbon in the small insertion domain and orange-yellow for sulphur. Sugar is coloured yellow for carbon; blue for nitrogen; and red for oxygen (c) The $2F_o - F_c$ OMIT electron density in the substrate-binding cleft of E315M, contoured at 1.0 σ. NAG5 (green) and NAG6 (yellow) are modelled into the density. NAG6 fits well into the density, however, residual unexplained density suggests a partial occupancy of the NAG5 conformation. (For interpretation of color mentioned in this figure the reader is referred to the web version of the article.)

tin polymer and in the bending process of long-chain chitooligomers.

Two additional residues (Tyr171 and Tyr435) are found at the edges of the catalytic cleft (Fig. 1b). Tyr171 appears to mark the non-reducing end of the hexasaccharide chain. Whereas, Trp435 marks the reducing end of the both the penta- and hexasaccharide chains (Fig. 2). Tyr435 located at the end of the +2 site seems to provide a partial barrier that may favour the ending of both sugar chains. However, inspection of the electron density map of the reducing-end subsites displays adequate space for the incoming oligomer to move beyond the +2 site, allowing various glycosidic bonds to approach the cleavage site. This explains how *V. harveyi* chitinase A hydrolyses a polymeric substrate in an endo manner at the same time favouring smaller substrates, such as hexaNAG (Suginta et al., 2005).

3.2. Specific interactions within the substrate-binding cleft of E315M

Fig. 3 depicts the relative positioning of the studied oligosaccharides inside the substrate-binding cleft of E315M. Four discernible sugar units of NAG5 (the GlcNAc residues in green) are bound to subsites −3, −2, +1, and +2, leaving the −1 site lying empty. NAG5 makes a number of interactions, either via hydrogen bonds (Fig. 2a) or via hydrophobic interactions, with residues in the substrate-binding cleft of E315M. As summarised in Table 2, five residues (Trp275, Lys370, Asp392, Trp397, and Tyr435) are directly involved in binding to +2NAG, whilst four residues (Trp275, Glu315 → Met, Asp392, and Arg463) contribute in binding to +1NAG and another five residues (Phe192, Gly274, Trp275, Glu498, and Trp570) to −2NAG. Specific interactions with −3NAG are made by Trp168, Arg173, Val205, Thr276, Trp497, and Glu498. The final non-reducing sugar of NAG5 could not be modelled into subsite −4 due to its poor electron density, probably reflecting a weak interaction in this conformation.

In relation to NAG5, NAG6 displays a more extensive set of interactions around the cleavage site extending to the reducing-end subsites (sites −1, +1, and +2) with its six sugar rings are entirely engaged with all the binding sites of E315M (the GlcNAc residues in yellow, Fig. 2b and 3a and b). Table 2 lists seven and six residues that participate in binding to +2NAG and +1NAG, respectively. These residues include all the residues that bind to NAG5, complemented by two extra (hydrophobic) interactions at each subsite (Phe316 and Gly367 at +2 site and Phe316 and Met389 at +1 site).

The mode of binding at the −1 site of E315M is particularly distinctive, since NAG6 interacts with twelve residues within this site, but there are no interactions with NAG5. To investigate further which conformation favours hydrolysis, the distances between the glycosidic oxygen and the OE1 atom of the γ-carboxyl side chain of catalytic Glu315 were estimated through superposition onto the wild-type structure. This distance is 2.98 Å for NAG6. The strained conformation of −1NAG combined with the twist of

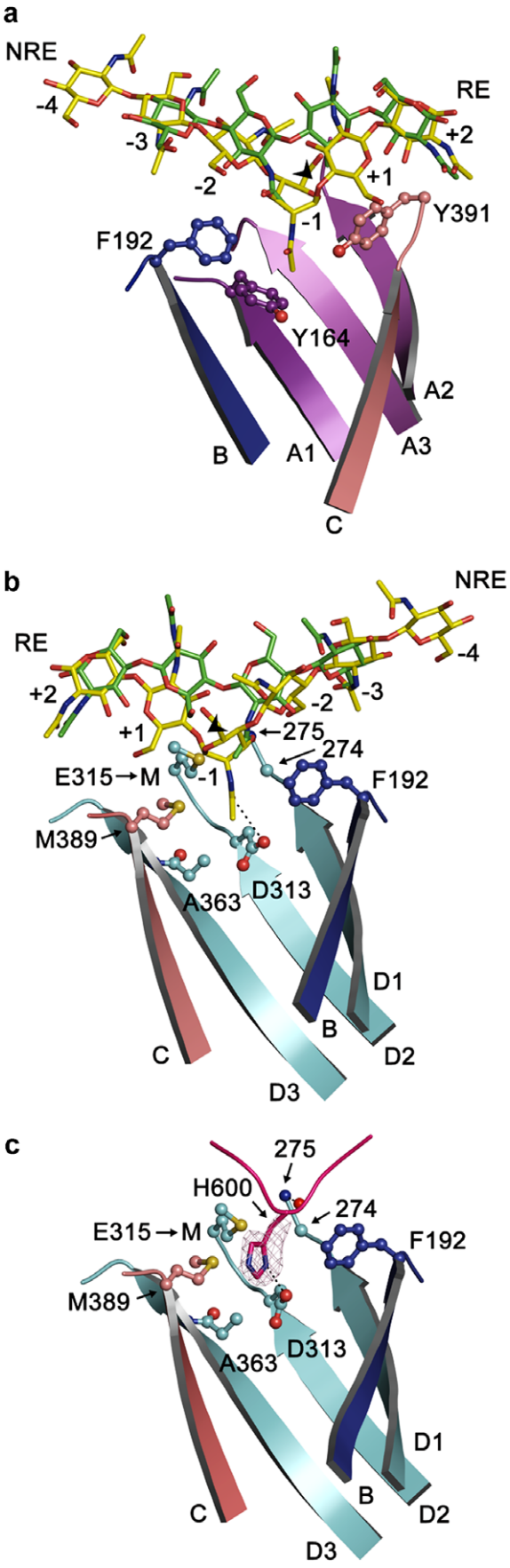

Fig. 3. A structural comparison of NAG_5 and NAG_6 in the catalytic cleft of E315M. (a) Superposition of E315M+NAG5 onto E315M+NAG6. Both sugars are shown along with interacting residues at the catalytic site. Only one protein chain is shown for clarity. (b) A 180° rotation of (a). Hydrogen bonds are shown as dashed lines (. . .). The eight β-strands are defined as A1 (residues 160–165); A2 (residues 455–460); A3 (residues 566–571); B (residues186–192); C (residues 384–389); D1 (residues 267–273); D2 (residues 308–313) and D3 (residues 358–366). Carbon atoms of the labeled amino acids are coloured purple for strands A1, A2, and A3; Blue for strand B; deep salmon for strand C; pale cyan for strands D1, D2, and D3. The binding residues are depicted as ball-and-stick models and orange-yellow for sulphur. An arrow indicates the cleavage site. NRE and RE represent non-reducing end and reducing end, respectively. (c) The $2F_o - F_c$ map of the His600 residue calculated from the final refined model and contoured at 1.0 σ. Atoms in the histidine residue are labeled pink for carbon; blue for nitrogen and red for oxygen.

Table 2
A summary of the interactions between NAG_5 and NAG_6 and the binding residues in the substrate-binding site of E315M

Binding subsites	E315M-binding residues[a]	
	pentaNAG	hexaNAG
+2	**Trp275**[b], **Lys370, Asp392, Trp397, Tyr435**	**Trp275,** Phe316, Gly367, **Lys370, Asp392, Trp397, Tyr435**
+1	**Trp275, Glu315 → Met, Asp392, Arg463**	**Trp275, Glu315 → Met,** Phe316, Met389, **Asp392, Arg463**
−1	Not observable	Tyr164, Phe192, Trp275, Asp313, Glu315 → Met, Ala363, Met389, Tyr391, Asp392, Tyr461, Arg463, Trp570
−2	**Phe192,** Gly274, **Trp275**, Glu498,**Trp570**	**Phe192, Trp275,** Thr276, **Trp570,** Glu571
−3	**Trp168, Arg173**, Val205, **Thr276, Trp497**, Glu498	**Trp168, Arg173, Thr276, Trp497**
−4	Not observable	Tyr171, Arg173, Trp497

[a] Direct contacts of each NAG with its adjacent residues were estimated, with the residues exhibiting a contact distance of ⩽4 Å being considered as binding residues.
[b] Residues in bold are shared between E315+NAG_5 and E315+NAG_6.

the bonds between −1NAG and +1NAG in the structure of NAG6 appear to present the scissile bond of NAG6 to the catalytic residue. However, the longer distance for NAG5 (5.06 Å) indicates that the position of the scissile linkage is too far away from Glu315 for hydrolysis to occur (see Fig. 3b), hence, a non-productive (non-hydrolysable) conformation is adopted by this sugar.

Fewer residues are engaged in coordination at the non-reducing end of NAG6 (four for −3NAG and three for −4 NAG) (Table 2). The larger number of contacts in the reducing-end binding sites probably reflects stronger interactions which may be of particular importance in defining the primary-binding sites for the incoming chitooligomer. Point mutations of Trp275 (binds to −1 and +1 NAG) and Trp397 (binds to +2 NAG), which caused a complete change in the cleavage patterns of the enzyme towards various chitoligosaccharides (Suginta et al., 2007), confirmed the binding-selectivity role of the reducing-end residues.

Most of the contacts for both NAG5 (orange, Fig. 2a) and NAG6 (magenta, Fig. 2b) involve the amino acid residues located within the catalytic domain. However, residues that belong to the α + β insertion domain also contact the substrates (Glu498, Tyr461, Arg463, and Trp497, green, Fig. 2a and b). Partial contribution of this domain to substrate binding was also noticeable in the complex of *S. marcescens* E315Q+NAG8 as described by Papanikolau et al. (2001).

Examination of the final structure of ligand-free E315M revealed that the catalytic cleft of the substrate-free enzyme is partially occupied by the six histidine affinity tag. These histidine residues are attached to the C-terminal end of a neighbouring chitinase molecule within the crystal and mimic the structure of the sugar rings. His600 particularly resembles −1NAG and makes most contact with the residues that bind to −1 NAG in the complex E315M+NAG6 (Fig. 3c).

3.3. Comparison of chitooligosaccharide-binding modes

The structures of the E315M complexes exhibited different conformations of NAG5 and NAG6. In addition to subsites −1 and +4 being unoccupied, the four sugar rings of NAG5 in the E315M+NAG5 complex do not fully lie on top of their corresponding sites in NAG6, with −2NAG and +1NAG (the sugar rings occupying the −2 and +1 subsites, respectively) being particularly displaced (Fig. 3a and b). As a result, the sugar oligomer may be expected to be interacting in a suboptimal manner. The glycosidic bond that joins −3NAG and −2NAG is twisted, causing the plane of −3NAG to lie perpendicular to the planes of the remaining sugars (Fig. 2a). Yet, the sugar chain maintains a linear form with no conversion of the chair configuration of any of the sugar residues. This linear confirmation may represent the initial step of binding, and therefore, it is referred to as the 'recognition' conformation.

A different substrate conformation is witnessed in the E315M+NAG6 complex. The $2F_o - F_c$ omit map (Fig. 2c) shows a full span of NAG6 through the −4 to +2 subsites and a twist of the glycosidic bond between −1NAG and +1NAG (rather than between −3NAG and −2NAG as observed for NAG5) (Fig. 2b). As a result, the planes of the reducing-end disaccharide (+1NAG and +2NAG) are rotated by 90 degrees from the original plane. Additionally, the NAG6 units assume a 'bent' conformation due to geometric constraints at the −1 site causing the sugar (−1NAG) unit to be pulled down by 4.45 Å. This bending event probably takes place as an outcome of the sliding of the sugar chain towards the immobilized reducing-end subsites, enabling the non-reducing-end unit to interact at subsite −4. This process most likely occurs through swapping hydrogen bonds to allow the orientations of the sugars to be maintained while introducing the kink into the backbone (compare Fig 2a to b). For much longer oligosaccharides the flexibility of ChBD with respect to the catalytic domain may aid this sliding mechanism, as illustrated in Fig. 1c.

The binding characteristics of E315M to NAG5 and NAG6 were studied by the fluorescence spectroscopy. Excitation at 295 nm produced ligand-dependent changes in fluorescence intensity at the maximum emission wavelength of 338 nm. The wavelength of this maximum was not altered by the presence of NAG5 or NAG6. The fluorescence intensities were found to be substrate concentration dependent and saturable, which typically represents ligand binding to the proteins (Fig. 4a). The fluorescence intensity data were fitted reasonably well into the single-site-binding model of a non-linear regression function (Fig. 4b). The estimated K_d values of mutant E315M and E315Q against NAG5 (0.72 ± 0.24 and 0.76 ± 0.23 μM) and NAG6 (0.09 ± 0.01 and 0.10 ± 0.01 μM) are found to be indistinguishable. This provides evidence that the different conformations of NAG5 and NAG6 detected in the active site of E315M (Fig. 2a and b) were not structural artifact due to increased hydrophobicity arising from the methionine substitution of Glu315. The K_d values of E315M/Q against NAG5 are estimated to be eight times higher than the values against NAG6. These values are a reflection of the fewer interactions of the linear NAG5, which we suggest represents the recognition conformation of an oligosaccharide. Sliding and bending of the oligosaccharide into the NAG6 conformation would result in an increase in the number of interactions and is consistent with a slower off rate contributing to an overall higher affinity.

3.4. Proposed catalytic mechanism

Inspection of the final $2F_o - F_c$ omit map of E315M+NAG6 shows good density throughout the NAG6 chain. However, there remains unexplained density unaccounted for by the NAG6 model. Comparison with the NAG5 structure suggests a lower occupancy conformation of the NAG6 in which the sugar follows the path of the NAG5 sugar (see Fig. 2c). Hence, NAG6 appears to adopt two conformations in binding to the mutant E315M, the major form being bent and the minor form linear.

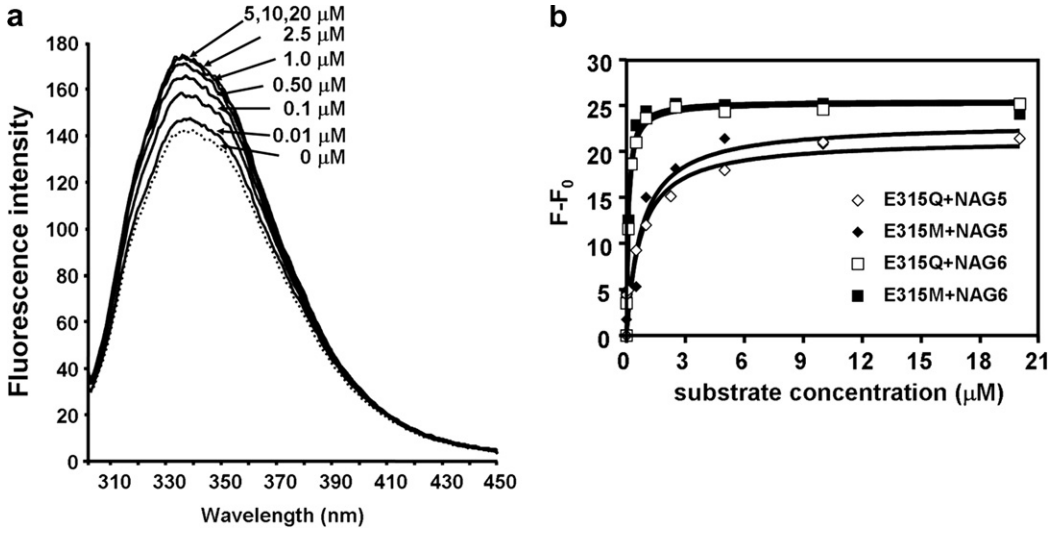

Fig. 4. Protein-ligand binding studies by fluorescence spectroscopy. (a) Effects of NAG_6 on the intrinsic fluorescence of E315M. Increased amounts of NAG_6 were added to 0.25 μM of the purified protein in 20 mM Tris–HCl (pH 8.0). The emission spectra were collected from 300–450 nm upon excitation of 295 nm. (b) The binding curves determined for NAG5 and NAG6 binding to mutants E315Q and E315M. Relative fluorescence intensity data ($F - F_o$) at 338 nm were fitted to a single-binding site model (see texts).

The distortion of −1NAG into a boat conformation and the twist of the scissile bond were predicted using molecular dynamics simulations (Brameld and Goddard, 1998a) and were verified by the crystal structures of *S. marcescens* chitobiase, hevamine, or *S. marcescens* ChiA (Aronson et al., 2003; Papanikolau et al., 2001; Terwisscha van Scheltinga et al., 1994; Tews et al., 1996; Tews et al., 1997). However, the partial density of the linear conformation in the electron density of NAG6 in E315M+NAG6 is the first crystallographic evidence for the occurrence of a recognition conformation that proceeds through a directed structural change to the catalytic conformation. Taking all the data obtained in this study together, *V. harveyi* chitinase A is presumed to catalyse the substrate hydrolysis following the 'slide and bend mechanism' as previously suggested for a long chain substrate (Watanabe et al., 2003). The proposed mechanism has four steps as shown in Fig. 5.

Step 1. *Substrate recognition:* A linear form of chitooligosaccharide enters the substrate-binding cleft and its reducing end (dark filled circle) is primarily recognised by the +2 binding residues, such as Trp275, Asp392, Trp397, and Tyr435 (Table 2).

Step 2. *Sliding and bending:* The sugar chain slides forward towards the reducing end distorting the chain especially in −1 NAG (green filled circle) and causing it to bend and take up a transient strained (boat) conformation. The increase in protein-sugar contacts in this conformation particularly in binding at the non-reducing end −4 site and at the catalytic site may drive this conformational change. Longer chitooligosaccharides may be aided in this movement by the flexibility in the ChBD relative to the catalytic domain.

Step 3. *Bond cleavage:* The twist of the scissile bond, together with the bending of −1NAG, renders the linking glycosidic oxygen accessible to the catalytic residue Glu315 for cleavage. The stereoselective attack of the reaction intermediate (oxazolinium ion) by a neighbouring water leads to a retention of configuration of the anomeric product (Papanikolau et al., 2001; Terwisscha van Scheltinga et al., 1994; Tews et al., 1997).

Step 4. *Product release:* The cleaved components have lower binding energy, permitting the oligosaccharide (mainly NAG2, dark-and blue- filled circles) at the product side to diffuse away.

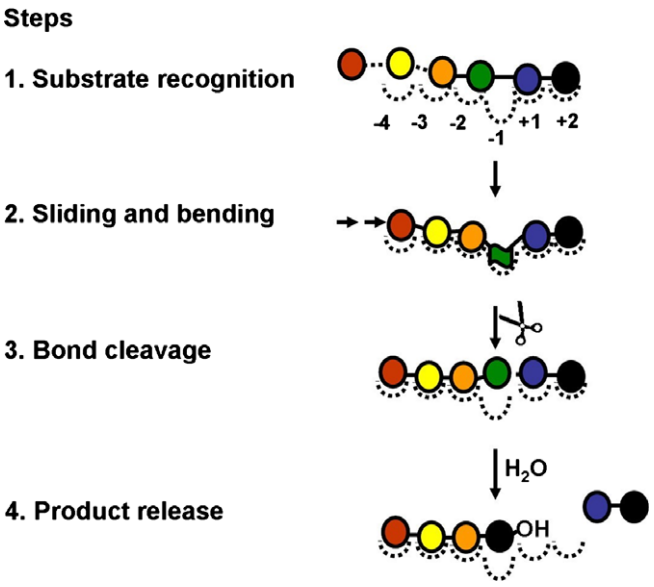

Fig. 5. The proposed catalytic mechanism of *V. carchariae* chitinase A. GlcNAc units are shown as filled, coloured circles. The reducing-end sugar is in black. Broken lines joining sugar rings represent free glycosidic bonds, solid lines depict constrained bonds. Curved dashed lines detail the binding subsites on the protein. Arrows signify the sliding of the sugar chain to allow the binding of the non-reducing end sugars (−4NAG) and for the green GlcNAc unit to adopt a boat conformation. (For interpretation of color mentioned in this figure the reader is referred to the web version of the article.)

4. Conclusions

This paper describes four crystal structures of *V. harveyi* chitinases A that have been solved to maximum resolution of 2.0–1.7 Å. The overall structure of chitinase A comprises three domains, which closely resembles chitinase A from *S. marcescens*. The structure of the ligand-free inactive mutant E315M displays blockage of the substrate-binding cleft by the C-terminal His6 residues from a second molecule. The structures of E315M bound to NAG5 and NAG6 provide key evidence that the interacting sugar undergoes conformational change to facilitate hydrolysis. Taking

all the data together, we propose that the *V. harveyi* chitinase A catalyses the hydrolytic reaction through a "slide and bend" mechanism.

Acknowledgments

This work is financially supported by The Thailand Research Fund (TRF) and The Thai Commission on Higher Education through Research Career Development Grant (RMU4980028), and the National Synchrotron Research Centre (NSRC), Thailand. R.C.R. and A.H.A. thank the Institute of Molecular and Cell Biology, Biopolis, Singapore and A*STAR, Singapore for their support.

References

Armand, S., Tomita, H., Heyraud, A., Gey, C., Watanabe, T., Henrissat, B., 1994. Stereochemical course of the hydrolysis reaction catalysed by chitinases A1 and D from *Bacillus circulans* WL-12. FEBS Lett. 343, 177–180.

Aronson Jr., N.N., Halloran, B.A., Alexyev, M.F., Amable, L., Madura, J.D., Pasupulati, L., Worth, C., van Roey, P., 2003. Family 18 chitinase-oligosaccharide substrate interaction: subsite preference and anomer selectivity of *Serratia marcescens* chitinase A. Biochem. J. 376, 87–95.

Bhattacharya, D., Nagpure, A., Gupta, R.K., 2007. Bacterial chitinases: properties and potential. Crit. Rev. Biotechnol. 27, 21–28.

Brameld, K.A., Goddard III., W.A., 1998a. Substrate distortion to a boat conformation at subsite −1 is critical in the mechanism of family 18 chitinases. J. Am. Chem. Soc. 120, 3571–3580.

Brameld, K.A., Goddard III., W.A., 1998b. The role of enzyme distortion in the single displacement mechanism of family 19 chitinases. Proc. Natl. Acad. Sci. USA 95, 4276–4281.

Bruce, A., Srinivasan, U., Staines, H.J., Highley, T.L., 1995. Chitinase and laminarinase production in liquid culture by *Trichoderma* spp. and their role in biocontrol of wood decay fungi. Int. Biodeterior. Biodegrad. 35, 337–353.

Collaborative Computational Project, Number 4., 1994. The CCP4 suit: programs for protein crystallography, Acta Crystallogr. D50, 760–763.

Srivastava, D.B., Ethayathulla, A.S., Kumar, J., Singh, N., Sharma, S., Das, U., Srinivasan, A., Singh, T.R., 2006. Crystal structure of a secretory signalling glycoprotein from sheep at 2.0 Å resolution. J. Struct. Biol. 156, 505–516.

Donnelly, L.E., Barnes, P.J., 2004. Acidic mammalian chitinase-a potential target for asthma therapy. Trends Pharmacol. Sci. 25, 509–511.

Fukamizo, T., 2000. Chitinolytic enzymes: catalysis, substrate binding, and their application. Curr. Protein Pept. Sci. 1, 105–124.

Fukamizo, T., Sasaki, C., Schelp, E., Bortone, K., Robertus, J.D., 2001. Kinetic properties of chitinase-1 from the fungal pathogen *Coccidioides immitis*. Biochemistry 40, 2448–2454.

Fusetti, F., von Moeller, H., Houston, D., Rozeboom, H.J., Dijkstra, B.W., Boot, R.G., Aerts, J.M., van Aalten, D.M., 2002. Structure of human chitotriosidase. Implications for specific inhibitor design and function of mammalian chitinase-like lectins. J. Biol. Chem. 277, 25537–25544.

Hart, P.J., Pfluger, H.D., Monzingo, A.F., Hollis, T., Robertus, J.D., 1995. The refined crystal structure of an endochitinase from *Hordeum vulgare* L. seeds at 1.8 Å resolution. J. Mol. Biol. 248, 402–413.

Hollis, T., Monzingo, A.F., Bortone, K., Ernst, S., Cox, R., Robertus, J.D., 2000. The X-ray structure of a chitinase from the pathogenic fungus *Coccidioides immitis*. Protein Sci. 9, 544–551.

Honda, Y., Kitaoka, M., Hayashi, K., 2004. Kinetic evidence related to substrate-assisted catalysis of family 18 chitinases. FEBS Lett. 567, 307–310.

Jeuniaux, C., 1961. Chitinase an addition to the list of hydrolases in the digestive tract of vertebrates. Nature 192, 135–136.

Jones, T.A., Zou, J.Y., Cowan, S.W., Kjeldgaard, M., 1991. Improved methods for building models in electron density maps and the location of errors in these models. Acta Crystallogr. A47, 110–119.

Kawada, M., Hachiya, Y., Arihiro, A., Mizoguchi, E., 2007. Role of mammalian chitinases in inflammatory conditions. Keio J. Med. 56, 21–27.

Keyhani, N.O., Roseman, S., 1999. Physiological aspects of chitin catabolism in marine bacteria. Biochim. Biophys. Acta 1473, 108–122.

Kuranda, M.J., Robbins, P.W., 1991. Chitinase is required for cell separation during growth of *Saccharomyces cerevisiae*. J. Biol. Chem. 266, 19758–19767.

Laemmli, U.K., 1970. Cleavage of structural proteins during assembly of head of bacteriophage T4. Nature 227, 680–685.

Laskowski, R.A., MacArthur, M.W., Moss, D.S., Thornton, J.M., 1993. PROCHECK: a program to check the stereochemical quality of protein structures. J. Appl. Crystallogr. 26, 283–291.

Leah, R., Tommerup, H., Svendsen, I., Mundy, J., 1991. Biochemical and molecular characterization of three anti-fungal proteins from barley seed. J. Biol. Chem. 266, 1564–1573.

Leslie, A.G.W., 1991. Recent changes to the MOSFLM package for processing film and image plate data. CCP4 and ESF-EACMB. Newsletters on Protein Crystallography. SERC Laboratory, Daresbury, Warrington, WA44AD, UK.

Li, Q., Wang, F., Zhou, Y., Xiao, X., 2005. Putative exposed aromatic and hydroxyl residues on the surface of the N-terminal domains of Chi1 from *Aeromonas caviae* CB101 are essential for chitin binding and hydrolysis. Appl. Environ. Microbiol. 71, 7559–7561.

Matsumoto, T., Nonaka, T., Hashimoto, M., Watanabe, T., Mitsui, Y., 1999. Three dimensional structure of the catalytic domain of chitinase A1 from *Bacillus circulans* WL-12 at a very high resolution. Proc. Jpn. Acad. 75, 269–274.

Murshudov, G.N., Vagin, A.A., Dodson, E.J., 1997. Refinement of macromolecular structures by the maximum-likelihood method. Acta Crystallogr. D53, 240–255.

Navaza, J., 1994. AmoRe: an automated package for molecular replacement. Acta Crystallog. Sect. A50, 157–163.

Pantoom, S., Songsiriritthigul, C., Suginta, W., 2008. The effects of the surface-exposed residues on the binding and hydrolytic activities of *Vibrio carchariae* chitinase A. BMC Biochem. 9 (2).

Papanikolau, Y., Prag, G., Tavlas, G., Vorgias, C.E., Oppenheim, A.B., Petratos, K., 2001. High resolution structural analyses of mutant chitinase A complexes with substrates provide new insight into the mechanism of catalysis. Biochemistry 40, 11338–11343.

Pedersen, K., Verdonck, L., Austin, B., Austin, D.A., Blanch, A.R., Grimont, P.A.D., Jofre, J., Koblavi, S., Larsen (IVP), J.L., Tiainen, T., Vigneulle, M., Swings, J., 1998. Taxonomic evidence that *Vibrio carchariae* Grimes et al. 1985 is a junior synonym of *Vibrio harveyi* (Johnson and Shunk 1936) Baumann et al.1981. Int. J. Syst. Bacteriol. 48, 749–758.

Perrakis, A., Tews, I., Dauter, Z., Oppenheim, A.B., Chet, I., Wilson, K.S., Vorgias, C.E., 1994. Crystal structure of a bacterial chitinase at 2.3 Å resolution. Structure 2, 1169–1180.

Robbins, P.W., Albright, C., Benfield, B., 1988. Cloning and expression of a *Streptomyces plicatus* chitinase (chitinase-63) in *Escherichia coli*. J. Biol. Chem. 263, 443–447.

Sahai, A.S., Manocha, M.S., 1993. Chitinases of fungi and plants: their involvement in morphogenesis and host–parasite interaction. FEMS Microbiol. 11, 317–338.

Sasaki, C., Yokoyama, A., Itoh, Y., Hashimoto, M., Watanabe, T., Fukamizo, T., 2002. Comparative study of the reaction mechanism of family 18 chitinases from plants and microbes. J. Biochem. (Tokyo) 131, 557–564.

Suginta, W., Robertson, P.A., Austin, B., Fry, S.C., Fothergill-Gilmore, L.A., 2000. Chitinases from *Vibrio*: activity screening and purification of chiA from *Vibrio carchariae*. J. Appl. Microbiol. 89, 76–84.

Suginta, W., Vongsuwan, A., Songsiriritthigul, C., Prinz, H., Estibeiro, P., Duncan, R.R., Svasti, J., Fothergill-Gilmore, L.A., 2004. An endochitinase A from *Vibrio carchariae*: cloning, expression, mass and sequence analyses, and chitin hydrolysis. Arch. Biochem. Biophys. 424, 171–180.

Suginta, W., Vongsuwan, A., Songsiriritthigul, C., Svasti, J., Prinz, H., 2005. Enzymatic properties of wild-type and active site mutants of chitinase A from *Vibrio carchariae*, as revealed by HPLC-MS. FEBS J. 272, 3376–3386.

Suginta, W., Songsiriritthigul, C., Kobdaj, A., Opassiri, R., Svasti, J., 2007. Mutations of Trp275 and Trp397 altered the binding selectivity of *Vibrio carchariae* chitinase A. Biochim. Biophys. Acta 1770, 1151–1160.

Suzuki, K., Taiyoji, M., Sugawara, N., Nikaidou, N., Henrissat, B., Watanabe, T., 1999. The third chitinase gene (chiC) of *Serratia marcescens* 2170 and the relationship of its product to other bacterial chitinases. Biochem. J. 343, 587–596.

Terwisscha van Scheltinga, A.C., Kalk, K.H., Beintema, J.J., Dijkstra, B.W., 1994. Crystal structures of hevamine, a plant defence protein with chitinase and lysozyme activity, and its complex with an inhibitor. Structure 2, 1181–1189.

Terwisscha van Scheltinga, A.C., Armand, S., Kalk, K.H., Isogai, A., Henrissat, B., Dijkstra, B.W., 1995. Stereochemistry of chitin hydrolysis by a plant chitinase/lysozyme and X-ray structure of a complex with allosamidin: evidence for substrate assisted catalysis. Biochemistry 34, 15619–15623.

Terwisscha van Scheltinga, A.C., Hennig, M., Dijkstra, B.W., 1996. The 1.8 Å resolution structure of hevamine, a plant chitinase/lysozyme, and analysis of the conserved sequence and structure motifs of glycosyl hydrolase family 18. J. Mol. Biol. 262, 243–257.

Tews, I., Perrakis, A., Oppenheim, A., Dauter, Z., Wilson, K.S., Vorgias, C.E., 1996. Bacterial chitobiase structure provides insight into catalytic mechanism and the basis of Tay-Sachs disease. Nat. Struct. Biol. 3, 638–648.

Tews, I., Terwisscha van Scheltinga, A.C., Perrakis, A., Wilson, K.S., Dijkstra, B.W., 1997. Substrate-assisted catalysis unifies two families of chitinolytic enzymes. J. Am. Chem. Soc. 119, 7954–7959.

Uchiyama, T., Katouno, F., Nikaidou, N., Nonaka, T., Sugiyama, J., Watanabe, T., 2001. Roles of the exposed aromatic residues in crystalline chitin hydrolysis by chitinase A from *Serratia marcescens* 2170. J. Biol. Chem. 276, 41343–41349.

Van Aalten, D.M., Synstad, B., Brurberg, M.B., Hough, E., Riise, B.W., Eijsink, V.G., Wierenga, R.K., 2000. Structure of a two-domain chitotriosidase from *Serratia marcescens* at 1.9-Å resolution. Proc. Natl. Acad. Sci. USA 97, 5842–5847.

Van Aalten, D.M., Komander, D., Synstad, B., Gaseidnes, S., Peter, M.G., Eijsink, V.G., 2001. Structural insights into the catalytic mechanism of a family 18 exo-chitinase. Proc. Natl. Acad. Sci. USA 98, 8979–8984.

Watanabe, T., Ishibashi, A., Ariga, Y., Hashimoto, M., Nikaidou, N., Sugiyama, J., Matsumoto, T., Nonaka, T., 2001. Trp122 and Trp134 on the surface of the catalytic domain are essential for crystalline chitin hydrolysis by *Bacillus circulans* chitinase A1. FEBS Lett. 494, 74–78.

Watanabe, T., Ariga, Y., Sato, U., Toratani, T., Hashimoto, M., Nikaidou, N., Kezuka, Y., Nonaka, T., Sugiyama, J., 2003. Aromatic residues within the substrate-binding cleft of *Bacillus Circulans* chitinase A1 are essential for hydrolysis of crystalline chitin. Biochem. J. 376, 237–244.

J Chem Biol
DOI 10.1007/s12154-009-0021-y

ORIGINAL ARTICLE

Substrate binding modes and anomer selectivity of chitinase A from *Vibrio harveyi*

Wipa Suginta · Supansa Pantoom · Heino Prinz

Received: 26 February 2009 / Accepted: 7 May 2009

Abstract High-performance liquid chromatography mass spectrometry (HPLC MS) was employed to assess the binding behaviors of various substrates to *Vibrio harveyi* chitinase A. Quantitative analysis revealed that hexaNAG preferred subsites −2 to +2 over subsites −3 to +2 and pentaNAG only required subsites −2 to +2, while subsites −4 to +2 were not used at all by both substrates. The results suggested that binding of the chitooligosaccharides to the enzyme essentially occurred in compulsory fashion. The symmetrical binding mode (−2 to +2) was favored presumably to allow the natural form of sugars to be utilized effectively. Crystalline α chitin was initially hydrolyzed into a diverse ensemble of chitin oligomers, providing a clear sign of random attacks that took place within chitin chains. However, the progressive degradation was shown to occur in greater extent at later time to complete hydrolysis. The effect of the reducing-end residues were also investigated by means of HPLC MS. Substitutions of Trp275 to Gly and Trp397 to Phe significantly shifted the anomer selectivity of the enzyme toward β substrates. The Trp275 mutation modulated the kinetic property of the enzyme by decreasing the catalytic constant (k_{cat}) and the substrate specificity (k_{cat}/K_m) toward all substrates by five- to tenfold. In contrast, the Trp397 mutation weakened the binding strength at subsite (+2), thereby speeding up the rate of the enzymatic cleavage toward soluble substrates but slowing down the rate of the progressive degradation toward insoluble chitin.

Keywords Chitin · Substrate binding mode · HPLC MS · *Vibrio harveyi* · Family-18 chitinase · Active-site mutation

Abbreviations

NAG_n	β-1-4 linked oligomers of *N*-acetylglucosamine residues where n=1–6
DNS	Dinitrosalicylic acid
IPTG	Isopropyl thio-β-D-galactoside
PMSF	Phenylmethylsulfonylfluoride
HPLC ESI-MS	High-performance liquid chromatography electrospray mass spectrometry
ChBD	Chitin-binding domain

Introduction

Chitin is a homopolymer composed of β-(1,4)-linked *N*-acetylglucosamine (GlcNAc or NAG) units and is mainly found as a structural component of fungal cell walls and exoskeletons of crustaceans and insects. A complete degradation of chitin requires chitinases (EC 3.2.1.14) and *N*-acetyl-β-glucosaminidases (EC 3.2.1.52). Chitinases are found in various organisms, and their physiological functions are dependent on the structural roles of chitin substrates existing in different species. Degradation of chitin by marine bacteria [1, 2] is crucial for maintaining the ecosystem in the marine environment [3]. In insects, chitinases are essential in the molting process and may also affect gut physiology through their involvement

W. Suginta (✉) · S. Pantoom
Biochemistry–Electrochemistry Research Unit,
School of Chemistry and Biochemistry, Institute of Science,
Suranaree University of Technology,
Nakhon, Ratchasima 30000, Thailand
e-mail: wipa@sut.ac.th

H. Prinz
The Max-Planck Institute of Molecular Physiology,
Otto-Hahn-Strasse 11,
44227 Dortmund, Germany

Published online: 28 May 2009

in peritrophic membrane turnover [4]. Plants produce chitinases as part of their defense mechanism against distinct pathogens [5, 6], whereas fungal chitinases participate in a number of morphogenetic processes, including spore germination, side-branch formation, differentiation into spores, and autolysis [7]. Human chitinases are involved in asthma and inflammatory conditions, but the endogenous substrate(s) and the pathogenic mechanism is not yet known [8–10].

Different bacteria seem to secrete different forms of chitinases [2, 11–17]. For example, *Serratia marcescens* produces three chitinases: ChiA, ChiB, and ChiC for a synergistic degradation of chitin [18, 19], whereas *Vibrio harveyi* (formerly *Vibrio carchariae*) mainly expresses chitinase A [2]. In the CAZy database (http://www.cazy.org), *V. harveyi* chitinase A is classified as a member of family-18 glycosyl hydrolases, comprising a $(\beta/\alpha)_8$-barrel catalytic domain with a deep substrate-binding cleft and is known to catalyze the hydrolytic reaction through the 'substrate-assisted' or 'retaining mechanism' [20–26]. Most recently, the crystal structures of *V. harveyi* chitinase and its mutant E315M complexed with NAG_5 and NAG_6 were reported at 1.8–2.1 Å resolutions [27]. The structures revealed that chitooligosaccharides most likely interact with the multiple subsites of the enzyme using a linear conformation. Subsequently, the sugar chain develops a 'kink' conformation to facilitate bond cleavage. Such a movement is presumed to proceed via the 'slide and bend' mechanism [27]. The sliding motion of a chitooligomer resembles the feeding mechanism proposed by Watanabe and co-workers [28] for long-chain chitin. Either sliding or feeding, the process could be achieved only when a chitinase exhibits high processivity toward its substrates. The processivity has been described previously for other polysaccharide degrading enzymes, such as Chi A from *S. marcescens* [19, 28–30], cellobiohydrolases Cel6A from *Humicola insolens* [31], and Cel7A from *Trichoderma reesei* [32].

Insoluble substrates have been proposed to enter the active site of chitinases by the feeding mechanism and chitin oligomers by a random mechanism [28, 33]. Such a hypothesis probably holds true for most of the cases. However, a major point of concern remains the random cleavage of a chitin polymer by an endo action of chitinase A. We previously verified that *V. harveyi* chitinase A initially degraded insoluble chitins into $NAG_{2\text{-}6}$ [20, 34]. Indeed, the production of the chitin oligomers other than NAG_2 cannot be explained as an outcome of the feeding mechanism. This is because the sliding following progressive degradation of chitin will only give rise to a single species of the product (NAG_2). In this study, we employed quantitative HPLC-MS as a direct and sensitive tool to investigate the binding behaviors of three different substrates. Together with kinetic analysis, we also demonstrated that point mutation of the reducing-end binding residues (Trp275 and Trp397) affected the substrate specificity of the tested substrates and significantly altered the anomer selectivity of *V. harveyi* chitinase A. This enzyme belongs to family-18 chitinases, which are potential drug targets for the treatment of allergic asthma.

Experimental

Bacterial strains and chemicals

The pQE 60 expression vector harboring the DNA fragment that encodes chitinase A (amino acid residues 22–597, without the 598–850 C-terminal fragment) and *Escherichia coli* type strain M15 (Qiagen, Valencia, CA, USA) were used for a high-level expression of recombinant chitinases. Chitooligosaccharides were obtained from Seikagaku Corporation (Bioactive Co., Ltd., Bangkok, Thailand). Flake chitin from crab shells was the product of Sigma-Aldrich Pte Ltd. (The Capricorn, Singapore Science Park II, Singapore). Other chemicals and reagents (analytical grade) were obtained from the following sources: reagents for bacterial media (Scharlau Chemie S.A., Barcelona, Spain.); all chemicals for protein preparation (Sigma-Aldrich Pte Ltd., Singapore and Carlo Erba Reagenti SpA, Limito, Italy); and reagents for HPLC-MS measurements (J.T. Baker, Deventer, Holland and LGC Promochem GmbH, Wesel, Germany). Milli-Q water was used for preparations of reaction buffers and for HPLC MS measurements.

Instrumentation

HPLC was operated on a 150×2.1 mm 5 μm Hypercarb®column (ThermoQuest, Thermo Electron Corporation, San Jose, CA, USA) connected to an Agilent Technologies 1100 series HPLC system (Agilent Technologies, Waldbronn, Germany) under the control of a Thermo Finnigan LTQ electrospray mass spectrometer. The proprietary program Xcalibur (Thermo Finnigan, Thermo Electron Corporation, San Jose, CA, USA) was used to control and calibrate HPLC ESI/MS. For partial hydrolysis of colloidal chitin, the electrospray MS was conducted under a positive full scan mode with a range of the mass/charge ratio (*m*/*z*) of 200–1,400. Later, the HPLC MS was run under the single ion monitoring mode for improvement of signal/noise ratios. The selected masses for detection were *m*/*z* 424.5 for NAG_2, *m*/*z* 627.5 for NAG_3, *m*/*z* 830.3 for NAG_4, *m*/*z* 1034.16 for NAG_5, and *m*/*z* 1236.3 for NAG_6. The UV signals were detected by a diode array detector between 200 and 400 nm.

Site directed mutagenesis

Point mutations were introduced to the wild-type *chitinase A* DNA that was previously cloned into the pQE60 expression vector by polymerase chain reaction (PCR) technique [20], using the QuickChange Site-Directed Mutagenesis Kit. Mutations of Trp275 to Gly and Trp397 to Phe (so as to create mutants W275G and W397F, respectively) were generated using oligonucleotides synthesized from BioServiceUnit (BSU) (Bangkok, Thailand) The forward oligonucleotide sequence used for mutagenesis of Trp275 to Gly is 5′-CATCTATCGGTGGTGGAACACTTTCTGAC-3′ and the reverse sequence is 5′-GTCAGAAAGTGTTCCACCACCGATAGATG-3′. For mutagenesis of Trp397 to Phe, the forward sequence is 5′-GACTTCTACGGCGGCTTCAACAACGTTCC-3′ and the reverse sequence is 5′-GGAACGTTGTTGAAGCCGCCGTAGAAGTC-3′. Sequences underlined represent the mutated codons. The success of point mutations was confirmed by automated DNA sequencing (BSU, Thailand).

Recombinant expression and purification

The wild-type chitinase A with a C-terminal hexahistidine sequence was highly expressed in *E. coli* M15 cells [20]. Chitinase A mutants W275G and W397F were obtained by PCR-based site directed mutagenesis as described by Suginta et al. [35]. For recombinant expression and purification, the freshly transformed cells were grown at 37 °C in 500 mL of Luria–Bertani medium containing 100 $\mu g \cdot mL^{-1}$ ampicillin until OD_{600} reached 0.6. Then, the chitinase production was induced by the addition of 0.5 mM IPTG at 25 °C for 18 h. The cell pellet was harvested by centrifugation, re-suspended in 40 mL of lysis buffer (20 mM Tris/HCl buffer, pH 8.0, containing 150 mM NaCl, 1 mM PMSF, and 1 $mg \cdot mL^{-1}$ lysozyme), and then lysed on ice using a Sonopuls Ultrasonic homogenizer with a 6-mm-diameter probe. The supernatant obtained after centrifugation at 12,000×*g*, 45 min was applied to a Ni-NTA agarose affinity column (1.0×10 cm) (Qiagen GmbH, Hilden, Germany), washed thoroughly with 5 mM imidazole, then eluted with 250 mM imidazole in 20 mM Tris/HCl buffer, pH 8.0. An eluted fraction (10 mL) was subjected to several rounds of membrane centrifugation using Vivaspin-20 ultrafiltration membrane concentrators (M_r 10,000 cut-off, Vivascience AG, Hannover, Germany) for a complete removal of imidazole and for concentrating the proteins. Protein purity was verified on sodium dodecyl sulfate polyacrylamide gel electrophoresis as described by Laemmli [36]. A final concentration of the protein was determined by Bradford's method [37] using a standard calibration curve of bovine serum albumin (0–25 μg). The freshly prepared proteins were subjected to functional characterization or stored at −30 °C.

Partial hydrolysis of chitooligosaccharides by *V. harveyi* chitinase A

Partial hydrolysis of chitooligosaccharides by wild-type was carried out in a 50-μL reaction mixture, containing 0.1 M ammonium acetate buffer, pH 7.0, 500 μM substrate, and 100 ng purified enzyme. To minimize isomerization of the anomeric products, the reaction was performed on ice (0 °C) for 3 min, and then a 10-μL aliquot was transferred to a 200-μL sample vial and immediately subjected to HPLC MS analysis. The sample tray was kept at 4 °C, and the column was operated at 10 °C. A constant flow rate of 0.4 $mL \cdot min^{-1}$ was applied with a run time set to 15 min using a 5–70% gradient of acetonitrile, containing 0.1% formic acid. The β/α ratios were calculated from the peak areas of the corresponding products using the program Xcalibur and applying an MS Genesis algorithm for peak detection.

Time courses of chitin hydrolysis

Time-course experiments were carried out on ice in a 100-μL reaction mixture, containing 0.1 M ammonium acetate buffer, pH 7.0, 10% (*w*/*v*) crystalline α chitin, and 50 ng purified enzyme. Aliquots of 10 μL were taken at 0, 3, 7, 20, 30, 60, and 180 min and analyzed immediately by HPLC MS as described for chitin oligosaccharides. The peak areas, which represent total ion counts of the hydrolytic products, were quantified using the program Xcalibur applying a MS Avalon algorithm for peak detection. Standard calibration curves of NAG moieties were constructed separately from a mixture of oligosaccharide containing 0.2–500 μM of $NAG_{1–6}$. These data points yielded a linear curve of each standard sugar with the R^2 values of 0.9995–1.0, thus allowing molar concentrations of chitooligosacharides to be determined with confidence. For the determination of β/α contents of the chitooligosaccharide products, the reaction mixture, containing 250 ng purified enzyme in 0.1 M ammonium acetate buffer, pH 7.0, was incubated with 500 μM NAG_5 or NAG_6. Aliquots of a 100-μL reaction mixture were taken at specified times and analyzed immediately by HPLC MS. Amounts of β and α anomers of the hydrolytic products were derived from the corresponding peak areas using the standard calibration curves constructed as mentioned above.

Steady-state kinetics

Kinetic measurements were determined in a microtiter plate using NAG_5, NAG_6, and colloidal chitin as substrates. A

reaction mixture (100 μL), containing 0–500 μM substrate and chitinase (50 μg wild type, 250 μg W275G, or 0.4 μg W397F) in 0.1 M sodium acetate buffer, pH 5.5 was incubated at 37 °C for 15 min. After boiling to 100 °C for 3 min, the entire reaction mixture was subjected to the reducing sugar assay using dinitrosalicylic acid (DNS) reagent as described by Miller [38]. For colloidal chitin, the reaction was carried out the same way as the reducing-sugar assay, but concentrations of colloidal chitin was varied from 0% to 5% (*w*/*v*) and amount of enzyme was used at 150 μg wild type, 700 μg W275G, or 200 μg W397F. The amounts of the reaction products were determined from a standard curve of NAG_2 (0–500 nmol). The kinetic values were evaluated from three independent sets of data using the nonlinear regression function available in GraphPad Prism version 5.0 (GraphPad Software Inc., San Diego, CA).

Results

Structural evidence of hexaNAG in the catalytic cleft of *V. harveyi* chitinase A

We recently described four crystal structures of *V. harveyi* chitinase A and its catalytically inactive mutant E315M in complex with chitooligosaccharides (PDB codes 3BS8, 3B9A, 3B90, and 3B9E) [27]. Figure 1a is a surface representation of the catalytic domain of the mutant E315M, displaying six units of NAG (yellow) being embedded inside a long, deep-binding groove and interact specifically with various aromatic residues that stretch along the elongated cleft of the enzyme. Figure 1b represents a stick model underlying specific interactions between Tyr171 and −4NAG, Trp168 and −3 NAG, Trp275 and Trp570 and −1 to +1NAG, and Trp397 and Tyr435 with +2NAG. It is clear that the hydrophobic faces of the residues Trp275 and Trp397 stack against the heterocyclic rings of the reducing-end sugar units (+1 NAG and +2NAG; blue, Fig. 1a, b). We previously suggested that both residues are important for the primary interaction with soluble substrates [35]. We shall discuss later, in this study, that Trp275 and Trp397 are also crucial for the progressive degradation of insoluble chitin.

The structure in Fig. 1b also displays the cleavage site that is located between sites −1 and +1 (red arrow). Following the retaining mechanism, further cleavage would be expected to yield only βNAG_4 and βNAG_2. The released NAG_4 had two fates. It may diffuse into the reaction mixture and then rebind or it may slide forward to accommodate the next cleavage if remained attached to the active site. On the other hand, NAG_2 would dissociate from the product side (+1 and +2) and serves as the end product of hydrolysis.

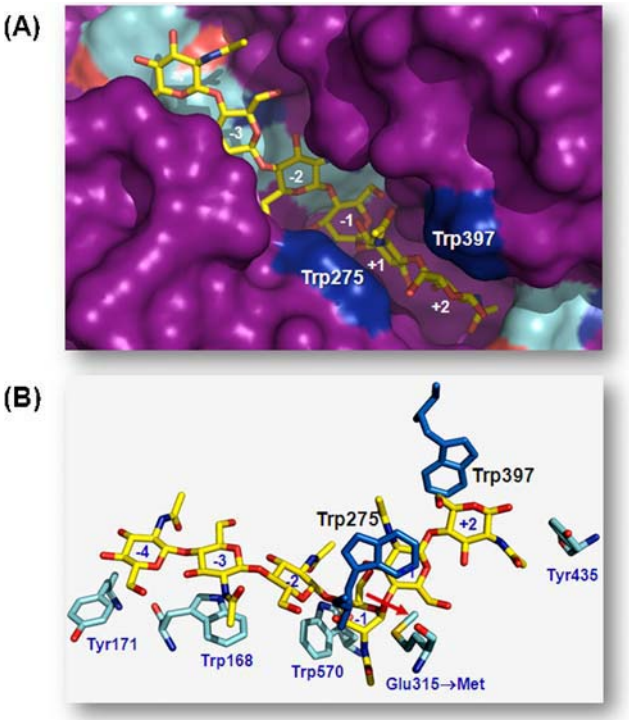

Fig. 1 The active site of *V. harveyi* chitinase A mutant E315M bound to hexaNAG. **a** A surface representation of hexaNAG that fully occupied subsites −4 to +2 within the substrate binding cleft of the enzyme. The sugar rings of NAG_6 are shown in *sticks*. **b** A stick model of the binding cleft of chitinase A mutant E315M complexed with NAG_6. N atoms are shown in *blue* and O atoms in *red*. C atoms are in *marine blue* for the amino acid residues and in *yellow* for the sugar residues. The cleavage site is indicated by an *arrow*, and Trp275 and Trp397 are represented in *blue*. The structure of E315M+NAG_6 complex is obtained from the PDB data base (PDB code, 3B9A) [24] and displayed by the program PyMol (http://www.pymol.org/)

Investigation of the binding modes of soluble substrates

We employed quantitative HPLC MS to establish the binding modes of three substrates. Pursuing the idea of Uchiyama et al. [28] that chitooligosaccharides randomly enter the catalytic cleft of chitinase A, it is presumed that binding of the incoming sugar chain may begin at variable sites to allow various glycosidic bonds to be accessible to the cleavage site located between sites −1 to +1. Figure 2a and b represent three possibilities where soluble substrates could interact with the multiple binding subsites of the enzyme. For a NAG_5 substrate, the binding may begin at site −4 and end at site +1, leading to a complete formation of βNAG_4+βNAG (Fig. 2a, bottom trace). Alternatively, the sugar chain may bind to subsites −3 to +2, subsequently generating βNAG_3+βNAG_2 (Fig. 2a, middle trace) or only four units of NAG_5 bind to subsites −2 to +2, leaving the reducing-end NAG unbound at the exterior of the substrate binding cleft. As a result, βNAG_2 and either equilibrium ratio of $\beta/\alpha NAG_3$ are expected (Fig. 2a, top trace).

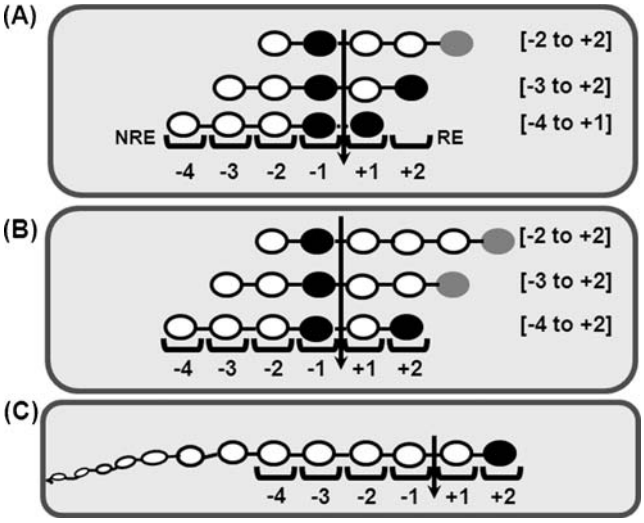

Fig. 2 Three possible models of chitin oligosaccharide bindings to the multiple binding subsites of *V. harveyi* chitinase A. Hydrolysis of **a** NAG_5, **b** NAG_6, and **c** crystalline α chitin. NAG unit with β configuration is shown in *black circle*, and NAG residue with α or β configuration with an equilibrium ratio is shown in *gray circle*. Types of the reducing-end anomers are predicted based on the retaining mechanism as suggested for family-18 chitinases

With respect to a NAG_6 substrate, it could interact with subsites (−4 to +2). This binding mode is seen in the structure of E315M+NAG_6, as shown in Fig. 1. The binding leads to a full occupancy of the six binding sites by chitohexaose (Fig. 2b, bottom trace). Subsequent bond cleavage results in the formation of βNAG_4+βNAG_2, where βNAG_2 is released from the reducing-end subsites +1 to +2. A different binding event takes place when five units of NAG_6 bind to positions (−3 to +2) (Fig. 2b, middle trace), leaving the reducing-end NAG lying empty beyond the substrate binding cleft. As a result, a single cleavage of NAG_6 leads to the formation of two NAG_3, one of which (the non-reducing end NAG_3) initially adopts β configuration, while the other NAG_3 possesses either β or α configuration. A third version of binding is that four units of NAG_6 symmetrically interact with subsites (−2 to +2), thereby letting the reducing-end NAG_2 remain unbound (Fig. 2b, top trace). This (−2 to +2) binding mode releases βNAG_2 from subsites (−2 and −1), whereas β or αNAG_4 is formed from the reducing-end side.

Assuming that the feeding mechanism is applicable, the binding characteristic of polymeric substrate is then depicted as Fig. 2c. After cleavage, a chitin chain remains attached to the active site before subsequently sliding forward toward the product side (+1 and +2), thereby allowing NAG_2 to be generated at a time. To investigate the preferred binding subsites of *V. harveyi* chitinase A, NAG_5 and NAG_6 (as a representative of soluble chitin) were partially hydrolyzed by the enzyme and the reaction mixtures analyzed immediately by HPLC MS. Partial hydrolysis of the two substrates was carried out at 0 °C to stabilize the β and α isomers of initial products. For the assignment of the HPLC elution of α and β anomers acquired by our system, we referred to a separation profile of chitooligosaccharides obtained by reverse-phase HPLC and ^{1}H-NMR [39]. Figure 3 represents an HPLC MS separation of chitin intermediates derived from partial hydrolysis of NAG_6. The β and α forms of an individual sugar were eluted at different retention times as a doublet. The preceding peak of the doublet is identified as β and the following peak α. Further mass detection by ESI-MS assigned *m/z* values of the two isomers of the same sugar to be identical. For instance, *m/z* 424.5 was seen for β/αNAG_2, 627.5 for β/αNAG_3, 830.3 for β/αNAG_4, and 1,236.5 for β&αNAG_6 (Fig. 3). Peak areas representing total ion counts of the corresponding oligomers were simply converted to molar concentrations using the standard calibration curves of $NAG_{1–6}$.

From Fig. 3, *V. harveyi* chitinase A degraded NAG_6, yielding βNAG_2+βNAG_3 as major isomers. This action was observed as early as 3 min. On the other hand, βNAG_4 and αNAG_4 were detected in comparable amounts, and NAG and NAG_5 were not observed at all (Fig. 3). With NAG_5 hydrolysis, two predominant products (βNAG_2 +αNAG_3) were captured during the initial time (data not shown). No other product was seen. The preferred binding modes of the enzyme toward NAG_5 and NAG_6 were determined by comparing β content to α content of the same product (Table 1). The β contents of NAG_2, NAG_3, and NAG_4 obtained from NAG_6 hydrolysis were estimated as 90%, 65%, and 46%, respectively (Table 1, wild type). Such values do not at all fit with the β/α ratios calculated by a single binding mode as presented in Fig. 2b. Apparently, the values agree well with the values (data in

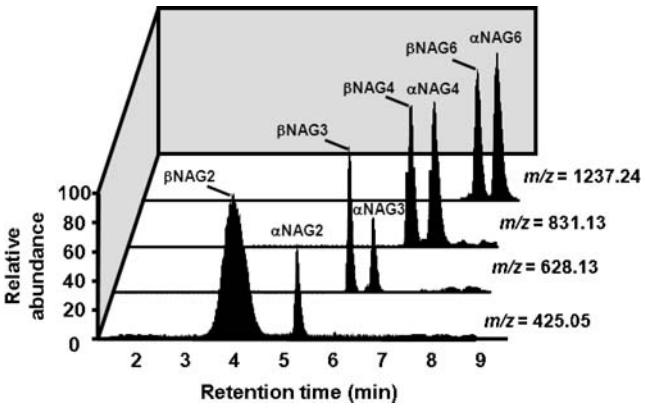

Fig. 3 An HPLC MS profile of the initial products obtained from partial hydrolysis of NAG6 by wild-type chitinase A. The hydrolytic reaction (50 μL) was carried out on ice to minimize the rate of mutarotation. After 3 min, aliquots of 10 μL of the reaction mixture were subjected to HPLC MS analysis

Table 1 Quantitative HPLC MS analysis of partial hydrolysis of chitooligosaccharides

Substrate	Enzyme	β content of initial products					
		NAG_1	NAG_2	NAG_3	NAG_4	NAG_5	NAG_6
pentaNAG (NAG5)	Wild-type	n.d.[a]	90±4.1(100)[b]	42±2.3(42)	n.d.	–	–
	W275G	n.d.	93±3.3	68±9.2	n.d.	–	–
	W397F	81±6.0	69±1.6	98±1.2	96±1.5	–	–
hexaNAG (NAG6)	Wild type	n.d.	90±2.2(100)[c]	65±3.0(71)	46±3.7(48)	–	–
	W275G	n.d.	92±4.9	63±0.7	79±2.8	–	–
	W397F	n.s.[d]	66±3.1	95±9.5	91±8.4	96±1.8	–
Crystalline α chitin	Wild type	n.d.	87±1.5(100)[e]	50±1.3(n.d.)	42±1.0(n.d)	37±0.9(n.d.)	46±4.5(n.d.)
	W275G	n.d.	88±1.2	48±2.2	56±3.2	49±5.8	50±3.7
	W397F	n.s.	88±2.1	46±1.2	57±3.4	57±1.4	51±2.0

A reaction mixture (50 μL), containing chitin substrates and chitinase A in 0.1 M ammonium acetate buffer, pH 7.0, was incubated on ice and then analyzed by HPLC ESI/MS after 3 min. The β contents were deduced from the peak areas of the corresponding products.

[a] n.d. represents product is not detectable

[b] The values in brackets are the expected values from the −2 to −2 binding mode for NAG5 hydrolysis

[c] The values in brackets are the expected values from a combination of the −3 to +2 and −2 to +2 modes for NAG6 hydrolysis

[d] n.s. represents non-separable between β and α anomer. The initial β contents were estimated from three independent sets of the experiment

[e] The value is predicted from the progressive degradation of insoluble chitin

brackets, Table 1) derived from a combination of the −2 to +2 and −3 to +2 binding modes (top and middle traces, Fig. 2b). For NAG_5 hydrolysis, the β contents of NAG_2 and NAG_3 products were predicted as 90% and 42%. These values are consistent with a single −2 to +2 binding mode (top trace, Fig. 2a). When the hydrolytic reactions were performed at equilibrium (25 °C, overnight), the predominating form of all the sugars was α. The equilibrium β contents were calculated as 48% for NAG_2, 42% for NAG_3, 41% for NAG_4, 39% for NAG_5, and 43% for NAG_6 (data not shown).

Substrate binding preference toward crystalline α chitin

The substrate binding mode of natural substrate was further investigated. Figure 4a represents a time course of the hydrolytic products generated from crystalline α chitin hydrolysis by the wild-type chitinase. Similar to previous findings [20, 34], NAG_6 was degraded by *V. harveyi* chitinase A, yielding NAG_2 major products. Other intermediates ($NAG_{3–6}$) were also detected in the reaction mixture as early as 3 min although in much lower concentrations. The major isomer of NAG_2 products was found to be β, while other products gave equilibrium ratios of α/β (Table 2). NAG_2 was released at least sevenfold greater than the other products over the entire range of reaction times (Fig. 4a), indicating that the enzymatic cleavage preferably took place at the second bond from the chain ends. Nevertheless, the peaks corresponding to $NAG_{3–6}$ that were detected in the reaction mixture simultaneously with NAG_2 verified the existence of a random attack occurring at internal points of a chitin chain.

The cleavage feature of a long-chain chitin was further elucidated. The values shown in Fig. 4b represent the cleavage ratios of NAG_2 to NAG_3–NAG_6. These values were compared when the reaction was carried out at initial time (3 min) and at equilibrium (180 min). In all cases, the cleavage ratios NAG_2 to other sugars were found to increase when the reactions reached equilibrium. For NAG_2/NAG_3, the ratio was enhanced by 1.5 times, for NAG_2/NAG_4 by nine times, for NAG_2/NAG_5 by five times, and for NAG_2/NAG_6 by six times. The lower cleavage ratios obtained at 3 min inferred that the internal attack proceeded at an early stage of reaction. The increased ratios represent the progressive action that took place at later time (i.e., at equilibrium).

Effects of point mutations on substrate bindings

Our recent data displayed a significant change in the cleavage patterns of NAG_4–NAG_6 hydrolysis when Trp275 was mutated to Gly and Trp397 to Phe. The 3D structure of chitinase A mutant E315M bound to NAG_6 has located Trp275 at the main subsites −1, and +1, and Trp397 at subsite +2 (Fig. 1a, b, blue). Alterations of the cleavage pattern as a result of Trp275 and Trp397 mutations provided a hint that both residues are important in defining the primary binding of soluble substrates [35]. In this study, we explored further how Trp275 and Trp397 influenced the binding selectivity of the enzyme. When incubated briefly,

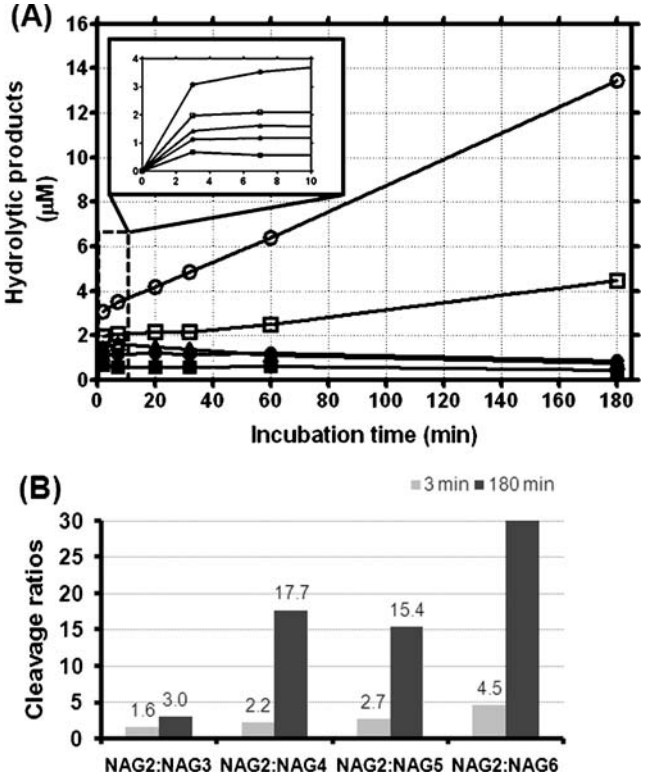

Fig. 4 Partial hydrolysis of crystalline α chitin by the wild-type chitinase A. **a** Time course of chitin hydrolysis. The hydrolytic reactions were carried out at on ice (0 °C) from 0 to 180 min and were analyzed immediately by HPLC MS. Molar concentrations of the hydrolytic products were estimated using the standard curves of NAG_{1-6}. **b** The cleavage ratios of NAG_2/NAG_{3-6} were calculated based on the molar concentration of each corresponding sugar. The reaction products generated during 0–10 min are indicated as an *inset*. *Open circle* dimers, *open square* trimers, *open triangle* tetramers; *filled circle* pentamers, *filled square* and hexamers

the mutant W275G was found to degrade NAG_5 into NAG_2 +NAG_3 with the value of βNAG_2 (93%) indistinguishable to the one formed by the wild-type enzyme (90%) (Table 1). However, the β content of NAG_3 (68%) produced by the mutated enzyme significantly increased when compared with the same product produced by the wild-type enzyme (42%). With mutant W397F, the initial products of NAG_5 hydrolysis by W397F were more varied from NAG to NAG_4. The major form of all the products produced by W397F was β with observed values of 81% for βNAG, 69% for βNAG_2, 98% for βNAG_3, and 96% βNAG_4 (Table 1).

Partial hydrolysis of NAG_6 by mutant W275G generated three product species (NAG_2+NAG_3+NAG_4), all having β major isomer. The percentages of βNAG_2 (92%) and βNAG_3 (63%) were not similar to the wild-type value (Table 1). However, βNAG_4 formed by W275G (79%) was significantly greater than βNAG_4 formed by wild type (46%). Similarly, NAG_6 hydrolysis by mutant W397F released a full range of reaction intermediates (NAG–NAG_5). The β contents for NAG_2 (66%), NAG_3 (95%), and NAG_4 (91%) were found to be different from that obtained from the non-mutated enzyme (Table 1).

Effects of point mutations on the kinetic properties

The steady-state kinetics of the hydrolytic activity of wild-type chitinase A and mutants W275G and W397F were investigated by using the DNS reducing-sugar assay (see "Experimental"). Table 2 represents the kinetic values of the three chitinase variants against NAG_5, NAG_6, and crystalline chitin. With NAG_5 hydrolysis, the K_m of W275G (315 μM) was only slightly decreased, but the K_m of W397F (476 μM) was 1.25-fold elevated from the K_m of wild type (380 μM). Similar results were observed with NAG_6 hydrolysis, where the K_m of W275G (238 μM) was twofold lower, whereas the K_m of W397F (460 μM) was 2.6-fold greater than the K_m of wild type (174 μM).

Mutations of Trp275 and Trp397exhibited a more severe effect on the catalytic constant (k_{cat}) of the enzyme. With the NAG_5 substrate, the k_{cat} of W275G (0.04 s^{-1}) was fivefold lower than that of wild type (0.21 s^{-1}). In contrast, the k_{cat} of W397F (2.1 s^{-1}) was tenfold higher. Similar results were seen with the NAG_6 substrate by which W275G (0.06 s^{-1}) showed a threefold decrease, but W397F displayed a 16-fold increase in the k_{cat} compared to that of wild type (0.19 s^{-1}).

Both mutations gave a different outcome on insoluble substrate. The K_m of W275G (25 mg mL^{-1}) and W397F (19 mg mL^{-1}) toward colloidal chitin were higher than that of wild type (12 mg mL^{-1}). Both mutants displayed a 0.3–0.5-fold loss in the k_{cat}. The k_{cat}/K_m values of W275G toward all substrates were decreased five times toward NAG_5 and NAG_6 but ten times toward the crystalline chitin. In contrast, the k_{cat}/K_m values of W397F toward the short-chain substrates were increased by six- to eightfold but a fivefold decrease toward the long-chain chitin.

Effects of point mutations on the anomer selectivity

The effects of Trp275 and Trp397 mutations on the anomer selectivity of the oligosaccharide hydrolysis were further investigated. Determination of substrate decrease at different time points revealed that the wild-type enzyme degraded both β and α anomers at equal rates (Fig. 5a). However, the initial rate of the depletion of βNAG_5 by W275G (Fig. 5a) occurred about 1.4 times faster than the rate of αNAG_5 depletion. At 155 min of incubation, only half of αNAG_5, but all of βNAG_5, was degraded. βNAG_5 was also utilized by mutant W397F at a significantly higher rate than αNAG_5; however, the anomer consumption varied linearly over time of incubation (Fig. 5b). At the end of reaction, a substantial amount of αNAG_5 (> 50%) and only

Table 2 Kinetic parameters of *V. harveyi* wild-type chitinase A and mutants

Chitinase A variants	pentaNAG			hexaNAG			Colloidal chitin		
	K_m (μM)	k_{cat} (s^{-1})	k_{cat}/K_m (s^{-1} μM^{-1})	K_m (μM)	k_{cat} (s^{-1})	k_{cat}/K_m (s^{-1} μM^{-1})	K_m (mg mL^{-1})	k_{cat} (s^{-1})	k_{cat}/K_m (s^{-1} (mg $mL^{-1})^{-1}$)
Wild type	380±49 (1)	0.21 (1)	5.5×10^{-4} (1)	174±23 (1)	0.19 (1)	11×10^{-4} (1)	12±1.4 (1)	0.10 (1)	83×10^{-4} (1)
W275G	315±110 (0.8)	0.04 (0.2)	1.3×10^{-4} (0.2)	238±17 (1.4)	0.06 (0.3)	2.5×10^{-4} (0.2)	25±3.7 (2.1)	0.02 (0.2)	8.0×10^{-4} (0.1)
W397F	476±11 (1.3)	2.1 (10)	44×10^{-4} (8)	460±53 (2.6)	3.0 (16)	65×10^{-4} (6)	19±0.1 (1.6)	0.03 (0.3)	16×10^{-4} (0.2)

Kinetic measurements of the hydrolytic activity of wild-type chitinase A and mutants W275G and W397F were carried out using 0–500 μM pentaNAG, hexaNAG and colloidal chitin as substrates. After 15 min of incubation at 37 °C, the amounts of the reaction products were determined by DNS assay using a standard curve constructed from NAG_2

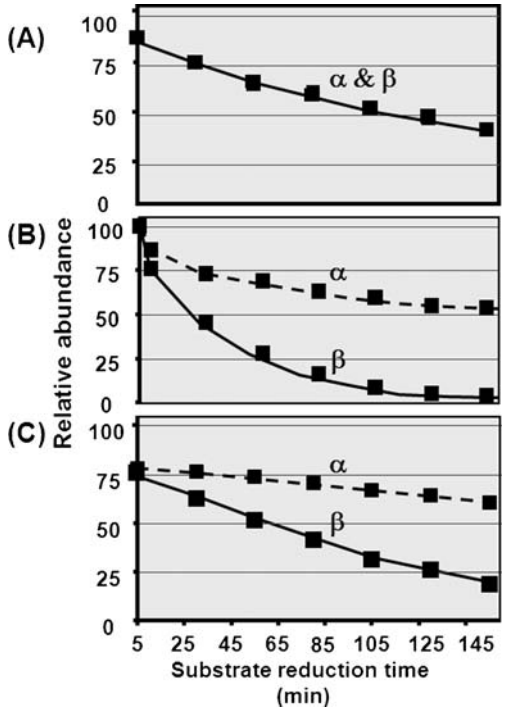

Fig. 5 Time-course of substrate consumption by chitinase A. Hydrolysis of NAG_5 by **a** wild type, **b** mutant W275G, and **c** mutant W397F. The hydrolytic reactions carried out at on ice (0 °C) from 0 to 155 min were analyzed by HPLC ESI/MS as described in texts. Rate of β anomer consumption is presented by a *black line* and rate of β anomer consumption by a *broken line*

a small amount of βNAG_5 (< 20%) remained in the reaction mixture.

With the NAG_6 substrate, similar patterns were observed (data not shown). The wild-type enzyme displayed no preferable selection toward a particular anomer of NAG_6. However, the initial rates of βNAG_6 degradation by both mutants were only slightly higher than that of αNAG_6 consumption. At the final stage of reaction, most of βNAG_5 and βNAG_6 (>80%) was used up.

Discussion

The 3D structures of the catalytically inactive mutant E315M complexed with NAG_5 and NAG_6 suggested that *V. harveyi* chitinase A most likely catalyzed chitin degradation through the 'slide and bend' mechanism [27]. From the mechanistic point of view, the sliding process can only be achieved by an enzyme with high processivity. Eijsink and colleagues reported previously that ChiA, ChiB, and ChiC from *S. marcescens* possessed different degrees of processivity [19, 29, 30]. ChiA was tested to be more processive than ChiB, whereas ChiC is a non-processive enzyme. The processive property explains how an enzyme processes it substrates. However, the mechanism

of how each substrate initially interacts with the enzyme depends entirely on the size of its substrate. Chitin oligomers are predicted to bind to the substrate-binding cleft by a random fashion. It implies that the sugar oligomer has freedom to bind to variable sites as far as the successful cleavage is concerned. In this study, three models are proposed for the productive binding of the soluble substrates (Fig. 1). NAG_5 may interact either with subsites (−4 to +1), (−3 to +2), or (−2 to +2) (Fig. 2a). Likewise, NAG_6 may bind to subsites (−4 to +2), (−3 to +2), or (−2 to +2) (Fig. 2b).

HPLC MS analysis of NAG_6 hydrolysis by wild-type chitinase gave rise to three species of reaction products ($NAG_{2,3,4}$). This happens only when the glycosidic cleavage takes place at least at two distinct locations. The presence of NAG_3 in the reaction mixture (Table 1) suggested that the enzymatic cleavage occurred in the middle of the chitin hexamer. When initial isomers of the degradation products were trapped at very low temperature (0 °C) for a short period of time (3 min), the estimated βNAG_3 (65%) agreed best to that of NAG_3 expected from the (−3 to +2) binding mode (71%) (the value in brackets, Table 1). Two other products (NAG_2 and NAG_4) could otherwise come from the interactions at subsites −4 to +2 or −2 to +2. However, the measured percentages of βNAG_2 (90%) and βNAG_4 (46%) were in conflict with the calculated values for the (−4 to +2) binding mode (100% for both βNAG_2 and βNAG_4). Instead, the obtained values agreed well with the 100% βNAG_2 and 48% βNAG_4 as calculated for the (−2 and +2) binding mode (Fig. 2b). This experimental outcome suggests binding of the chitin hexamer to either subsites −3 to +2 or −2 to +2, which emphasizes a dynamic process of interaction between an active enzyme and the substrate, and is in contrast with the occupation of the oligomer as observed in the static complex of the inactive enzyme (Fig. 1a, b). Previous quantitative HPLC MS analysis estimated the yield of NAG_3 to be 4 nmol when NAG_6 was incubated with native chitinase A for 5 min. This yield was half of NAG_2+NAG_4 yields (~8 nmol) obtained from the same reaction [34], and it indicated that NAG_6 favors the (−2 to +2) mode over the (−3 to +2) mode.

Limited hydrolysis of NAG_5 yielded only two products (NAG_2+NAG_3), meaning that the bond cleavage took place only at a single site either at positions −3 to +2 or –2 to +2 (see Fig. 2A). However, the observed percentages of βNAG_2 (90%) and βNAG_3 (42%) agreed more to that of βNAG_2 (100%) and βNAG_3 (42%) predicted for the (−2 to +2) binding mode. In contrast, 100% βNAG_2 and 100% βNAG_3 would be expected from the (−3 to +2) binding mode. No detection of NAG and NAG_4 in the reaction mixture implied that the (−4 to +1) mode was completely ignored by this substrate (see Table 1).

The binding characteristics of *S. marcescens* Chi A [40] and *Coccidioides immitis* chitinase-1 (CiX1) [41] were previously investigated by means of typical HPLC systems. Hydrolysis of NAG_6 by SmChiA that yielded 99% βNAG_2, 71% βNAG_3 and 48% βNAG_4 and hydrolysis of NAG_5 that yielded 100% βNAG_2 and 55% βNAG_3 represents the equivalent binding events as observed in this study. In CiX1, formations of $\alpha/\beta NAG_2$ (9/1) and α/βNAG4 (5/2) from NAG6 hydrolysis supports the (-2 to +2) binding mode. Sasaki et al. [42] performed a comparative study of the reaction mechanism of rice and bacterial enzymes and concluded that microbial chitinases favors the (−2)(−1)(+1)(+2)(+3)(+4) subsites, while plant chitinases prefers the (−4)(-3)(−2)(−1)(+1)(+2) subsites. Binding of a chitooligomer to (−2) to (+4) sites would be comparable to the −2 to +2 binding mode described for *V. harveyi* chitinase A.

With partial hydrolysis of insoluble chitin, NAG_2 observed as the primary product during the course of reaction (from 0 to 180 min) was mostly derived from the progressive degradation of the second bond from a chain end of chitin polymer. Imai et al. [33] demonstrated previously that the degradation of β chitin microfibrils took place from the reducing end of the sugar chain. However, other products ($NAG_{3–6}$) that were observed in the reaction mixture, even as early as 3 min, and the equilibrium ratios of $NAG_{3–6}$ products obtained from a long-chain chitin hydrolysis (Table 1) were an indication of internal attacks that took place at variable positions within the chitin chain. This interpretation is further supported by the small cleavage ratios of $NAG_2/NAG_{3–6}$ intermediates. A dramatic increase in the ratios at later time of reaction is presumably achieved quite productively with the progressive action via the feeding and sliding mechanism.

The anomer analysis revealed no selectivity of the wild-type chitinase A in utilization of α or β substrates (Fig. 5a). No selectivity of binding by all means leaves the enzyme a lot more freedom to efficiently take up the β or α substrates that are present in the reaction equilibrium. This idea is well complimented by binding of NAG_5 to subsites (−2 to +2) and NAG_6 to subsites (−3 to +2) or (−2 to +2) as seen in Fig. 2a and b. For the structural point of view, *V. harveyi* chitinase A is shown to comprise a substrate binding cleft with a long, deep groove structure (Fig. 1). The reducing end of the binding groove is shown to be open, giving adequate space for the incoming sugar chain to move beyond the +2 site. As a consequence, various glycosidic bonds are accessible to the cleavage site. The open-end active site certainly fits the binding preference of NAG_5 and NAG_6 and the endo action of the enzyme toward chitin polymers.

We previously reported that the residues Trp275 and Trp397 positioned at subsites (−1, +1, and +2 sites) are particularly essential for defining the primary binding of

soluble chitooligosaccharides and Trp70 located at the N-terminal end of the ChBD is crucial for insoluble chitin degradation [35, 43]. In this study, the effects of mutations on the kinetic properties of the enzyme were evaluated. It was found that mutations of Trp275 and Trp397 to Gly and Phe, respectively, significantly changed the substrate specificity and the anomer selectivity of the enzyme. The structure of mutant E315M bound to NAG_6 showed that Trp275 could interact strongly with −1NAG and +1NAG [27]. Mutation of this residue was found to affect the kinetic properties involving the catalytic center by decreasing the k_{cat} and the k_{cat}/K_m toward NAG_5 and NAG_6 by a magnitude of 5 (Table 2). In addition, the mutation significantly increased the apparent rate of β consumption as shown in Fig. 5a. The event may be explained as a shift of the sugar chain toward the non-reducing end in the search for other available binding sites to compensate for the loss of interactions. The observed yields of βNAG_2 (93%) and βNAG_3 (68%) obtained from the cleavage of NAG_5 by W275G (Table 1) agrees well with the predicted yields of βNAG_2 (100%) and βNAG_3 (42–100%) of the model shown in Fig. 6a. A single move of the sugar chain toward the non-reducing end is predicted as further movement would likely be blocked by high affinity of binding between the reducing end of NAG_5 and Trp397 at subsite +2.

Different situations were observed with mutant W397F. Mutation of Trp397 to Phe led to an increase in the k_{cat} toward NAG_5 and NAG_6 by 10- and16-fold, giving rise to an increase in the k_{cat}/K_m by a magnitude of 8 and 16, respectively. Trp397 is a crucial binding residue located at subsite +2, and it determines the primary binding of chitooligosaccharide substrates. A phenylalanine substitution appeared to weaken the binding strength of this subsite, enabling the sugar chain to move more freely and allowing various glycosidic bonds to be exposed to the cleavage sites. A full range of reaction intermediates seen in the reaction mixture of W397F (Table 1) supports the above assumption. Hydrolysis of NAG_5 by W397F, yielding 81% βNAG, 69% βNAG_2, 98% βNAG_3, and 96% βNAG_4 products agreed well with the yields proposed in Fig. 6b.

The residues Trp275 and Trp397 are found to be important for insoluble chitin hydrolysis, since the mutations showed a remarkable decrease in the k_{cat} value of the enzyme. The structure in Fig. 1 shows that both residues are located in a perfect position to be responsible for the feeding process by pulling the chitin chain toward the reducing end subsites, thereby permitting the next processive hydrolysis to occur (see Fig. 6c). A significant reduction of the k_{cat} and the k_{cat}/K_m values toward colloidal chitin (Table 2) seems to support the proposed roles of both residues (Table 2). Similar effects were also reported with ChiA1 from *B. circulans*, where mutations of Trp164 (equivalent to Trp275) and Trp285 (equivalent to Trp397) drastically reduced the hydrolytic activity of their enzymes toward colloidal chitin by 40–50% [44].

In conclusion, we employed quantitative HPLC MS to determine the binding modes of a family-18 chitinase from *V. harveyi* toward three substrates. Neither a random nor a progressive binding was entirely employed for a complete hydrolysis of the tested substrates. Nevertheless, soluble chitins seem to favor the −2 to +2 binding, but insoluble chitin preferred the progressive binding. Mutations of Trp275 and Trp397 were found to affect the anomer selectivity and the substrate specificity toward soluble substrates. The evaluation of the kinetic data suggested

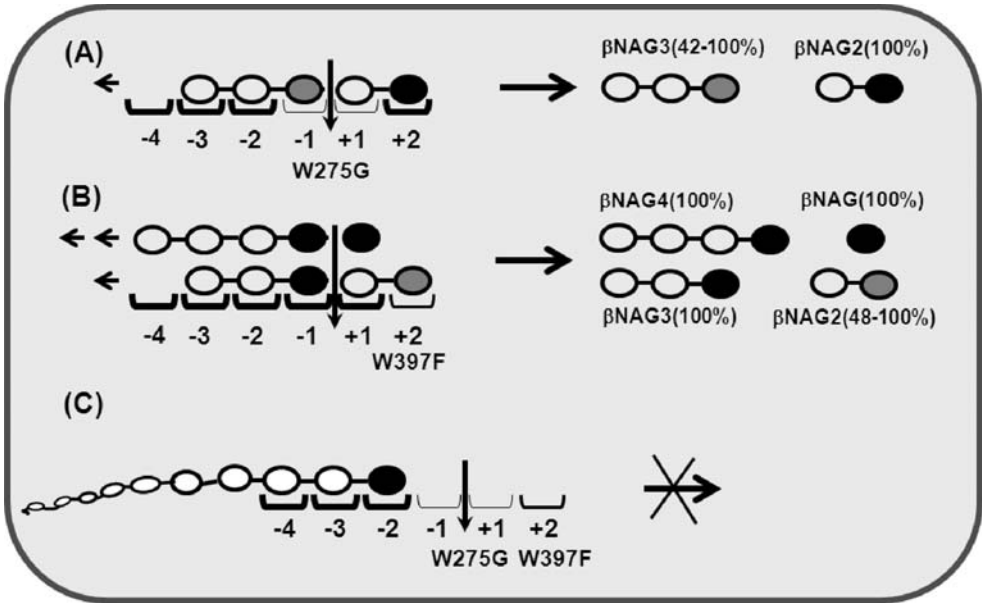

Fig. 6 Plausible effects of point mutation on the substrate binding preference and the anomer selectivity. Binding of NAG_5 to **a** wild-type chitinase, **b** mutant W275G, and **c** mutant W397F. The β configuration is shown in *black circle*, NAG residue with α or β configuration with an equilibrium ratio is shown in *gray circle*, and NAG residue with α or β configuration that binds to a loosen-affinity binding site is shown in *gray-filled in dark circle*. The cleavage site is indicated by an *arrow*

that Trp275 and Trp397 are likely involved in the feeding process that facilitates a degradation of chitin polymer in a progressive manner. Ultimately, understanding of the binding mechanism of family-18 chitinases to their substrates may aid the drug-screening program to obtain effective inhibitors that act as therapeutic candidates for successful treatment of allergic asthma.

Acknowledgements This work is financially supported by Suranaree University of Technology, The Thailand Research Fund and The Thai Commission on Higher Education through a Research Career Development Grant to WS (grant no. RMU4980028). The Thailand Research Fund through the Royal Golden Jubilee PhD Program (grant no. PHD/0238/2549) to SP and WS is acknowledged.

References

1. Hirono I, Yamashita M, Aoki T (1998) Note: molecular cloning of chitinase genes from *Vibrio anguillarum* and *V. parahaemolyticus*. J Appl Microbiol 84:1175–1178
2. Suginta W, Robertson PA, Austin B et al (2000) Chitinases from *Vibrios*: activity screening and purification of chi A from *Vibrio carchariae*. J Appl Microbiol 89:76–84
3. Keyhani NO, Roseman S (1999) Physiological aspects of chitin catabolism in marine bacteria. Biochim Biophys Acta 1473:108–122
4. Merzendorfer H, Zimoch L (2003) Chitin metabolism in insects: structure, function and regulation of chitin synthases and chitinases. J Exp Biol 206:4393–4412
5. Herrera-Estrella A, Chet I (1999) Chitinases in biological control. EXS 87:171–184
6. Melchers LS, Stuiver MH (2000) Novel genes for disease-resistance breeding. Curr Opin Plant Biol 3:147–152
7. Gooday GW, Zhu WY, O'Donnell RW (1992) What are the roles of chitinases in the growing fungus? FEMS Microbiol Lett 100:387–392
8. Wills-Karp M, Karp CL (2004) Chitin checking—novel insights into asthma. N Engl J Med 351:1455–1457
9. Kawada M, Hachiya Y, Arihiro A et al (2007) Role of mammalian chitinases in inflammatory conditions. Keio J Med 56:21–27
10. Zhu Z, Zheng T, Homer RJ et al (2004) Elias acidic mammalian chitinase in asthmatic Th2 inflammation and IL-13 pathway activation. Science 304:1678–1682
11. Watanabe T, Suzuki K, OyaGi W et al (1990) Gene cloning of chitinase A1 from *Bacillus circulans* WL-12 revealed its evolutionary relationship to *Serratia* chitinase and to the type III homology units of fibronectin. J Biol Chem 265:15659–15665
12. Jones JDG, Grady KL, Suslow TV et al (1986) Isolation and characterization of genes encoding two chitinase enzymes from *Serratia marcescens*. EMBO J 5:6467–6473
13. Roffey PE, Pemberton JM (1990) Cloning and expression of an *Aeromonas hydrophila* chitinase gene in *Escherichia coli*. Curr Microbiol 21:329–337
14. Sitrit Y, Vorgias CE, Chet I et al (1995) Cloning and primary structure of The chiA gene from *Aeromonas caviae*. J Bacteriol 177:4187–4189
15. Tsujibo H, Orikoshi H, Tanno H et al (1993) Cloning, sequence, and expression of a chitinase gene from a marine bacterium, *Altermonas sp.* strain O-7. J Bacteriol 175:176–181
16. Suginta W (2007) Identification of chitin binding proteins and characterization of two chitinase isoforms from *Vibrio alginolyticus* 283. Enzyme Microb Tech 41:212–220
17. Itoi S, Kanomata Y, Koyama Y et al (2007) Identification of a novel endochitinase from a marine bacterium *Vibrio proteolyticus* strain No. 442. Biochim Biophys Acta 1774:1099–1107
18. Suzuki K, Sugawara N, Suzuki M et al (2002) Chitinases A, B, and C1 of *Serratia marcescens* 2170 produced by recombinant *Escherichia coli:* enzymatic properties and synergism on chitin degradation. Biosci Biotechnol Biochem 66:1075–1083
19. Sikorski P, Sørbotten A, Horn SJ et al (2006) *Serratia marcescens* chitinases with tunnel-shaped substrate-binding grooves show endo activity and different degrees of processivity during enzymatic hydrolysis of chitosan. Biochemistry 45:9566–9574
20. Suginta W, Vongsuwan A, Songsiriritthigul C et al (2004) An endochitinase A from *Vibrio carchariae*: cloning, expression, mass and sequence analyses, and chitin hydrolysis. Arch Biochem Biophys 424:171–180
21. Perrakis A, Tews I, Dauter Z et al (1994) Crystal structure of a bacterial chitinase at 2.3 Å resolution. Structure 2:1169–1180
22. Tews I, Terwisscha van Scheltinga AC, Perrakis A et al (1997) Substrate assisted catalysis unifies two families of chitinolytic enzymes. J Am Chem Soc 119:7954–7959
23. Terwisscha van Scheltinga AC, Armand S, Kalk KH et al (1995) Stereochemistry of chitin hydrolysis by a plant chitinase/lysozyme and X-ray structure of a complex with allosamidin: evidence for substrate assisted catalysis. Biochemistry 34:15619–15623
24. Hollis T, Monzingo AF, Bortone K et al (2000) The X-ray structure of a chitinase from the pathogenic fungus *Coccidioides immitis*. Protein Sci 9:544–551
25. Brameld KA, Goddard WA III (1998) Substrate distortion to a boat conformation at subsite -1 is critical in the mechanism of family 18 chitinases. J Am Chem Soc 120:3571–3580
26. Terwisscha van Scheltinga AC, Hennig M, Dijkstra BW (1996) The 1.8 Å resolution structure of hevamine, a plant chitinase/lysozyme, and analysis of the conserved sequence and structure motifs of glycosyl hydrolase family 18. J Mol Biol 262:243–257
27. Songsiriritthigul C, Pantoom S, Aguda AH et al (2008) Crystal structures of *Vibrio harveyi* chitinase A complexed with chitooligosaccharides: implications for the catalytic mechanism. J Struct Biol 162:491–499
28. Uchiyama T, Katouno F, Nikaidou N et al (2001) Roles of the exposed aromatic residues in crystalline chitin hydrolysis by chitinase A from *Serratia marcescens* 2170. J Biol Chem 276:41343–41349
29. Sørbotten A, Horn SJ, Eijsink VG et al (2005) Degradation of chitosans with chitinase B from *Serratia marcescens.* Production of chitooligosaccharides and insight into enzyme processivity. FEBS J 272:538–549
30. Horn SJ, Sørbotten A, Synstad B et al (2006) Endo/exo mechanism and processivity of family 18 chitinases produced by *Serratia marcescens*. FEBS J 273:491–503
31. Boisset C, Fraschini C, Schülein M et al (2000) Imaging the enzymatic digestion of bacterial cellulose ribbons reveals the endo character of the cellobiohydrolase Cel6A from *Humicola insolens* and its mode of synergy with cellobiohydrolase Cel7A. Appl Environ Microbiol 66:1444–1452
32. Imai T, Boisset C, Samejima M et al (1998) Unidirectional processive action of cellobiohydrolase Cel7A on Valonia cellulose microcrystals. FEBS Lett 432:113–116
33. Imai T, Watanabe T, Yui T, Sugiyama J (2002) Directional degradation of beta-chitin by chitinase A1 revealed by a novel reducing end labelling technique. FEBS Lett 510:201–205
34. Suginta W, Vongsuwan A, Songsiriritthigul C et al (2005) Enzymatic properties of wild-type and active site mutants of chitinase A from *Vibrio carchariae*, as revealed by HPLC-MS. FEBS J 272:3376–3386

35. Suginta W, Songsiriritthigul C, Kobdaj A et al (2007) Mutations of Trp275 and Trp397 altered the binding selectivity of *Vibrio carchariae* chitinase A. Biochim Biophys Acta 1770:1151–1160
36. Laemmli UK (1970) Cleavage of structural proteins during the assembly of the head of bacteriophage T4. Nature 227:680–685
37. Bradford MM (1976) A rapid and sensitive method for the quantitation of microgram quantities of protein utilizing the principle of protein-dye binding. Anal Biochem 72:248–254
38. Miller GL (1959) Use of dinitrosalicylic acid reagent for determination of reducing sugar. Anal Chem 31:426–429
39. Armand S, Tomita H, Heyraud A et al (1994) Stereochemical course of the hydrolysis reaction catalysed by chitinase A1 and D from *Bacillus circulans* WL-12. FEBS Lett 343:177–180
40. Aronson NN Jr, Halloran BA, Alexyev MF et al (2003) Family 18 chitinase-oligosaccharide substrate interaction: subsite preference and anomer selectivity of *Serratia marcescens* chitinase A. Biochem J 376:87–95
41. Fukamizo T, Sasaki C, Schelp E et al (2001) Kinetic properties of chitinase-1 from the fungal pathogen *Coccidioides immitis*. Biochemistry 40:2448–2454
42. Sasaki C, Yokoyama A, Itoh Y et al (2002) Comparative study of the reaction mechanism of family 18 chitinases from plants and microbes. J Biochem 131:557–564
43. Pantoom S, Songsiriritthigul C, Suginta W (2008) The effects of the surface-exposed residues on the binding and hydrolytic activities of *Vibrio carchariae* chitinase A. BMC Biochem 9:2
44. Watanabe T, Ariga Y, Sato U et al (2003) Aromatic residues within the substrate-binding cleft of *Bacillus circulans* chitinase A1 are essential for hydrolysis of crystalline chitin. Biochem J 376:237–244